DYNAMICS OF THE SPINNING TOP: DISCRETIZATION AND INTERACTIVE VISUALIZATION

Diploma Thesis

by
René Bodack

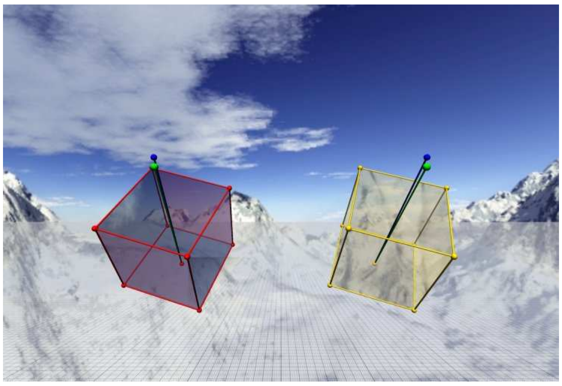

Technische Universität Berlin
Institut für Mathematik

Prof. A. I. Bobenko

Berlin, August 18, 2008

Die selbstständige und eigenhändige Anfertigung
versichere ich an Eides statt.

Berlin, 18. August 2008

Contents

Chapter 1

Introduction

The spinning top, a rigid body moving around a fixed point in a homogeneous gravity field, is a famous topic in classical mechanics. Its non-linear equations of motion are the well known Kirchhoff equations, whose discretization and hence actual calculation is topic of the present work. In order to achieve quality path discretizations it is advisable to use all present knowledge of the mechanical system, e. g. the fact that they preserve their energy, and hence have a so called integral of motion. Yet the Kirchhoff equations have only two such integrals, so they are not integrable and there is no integrable discretizations as well. There are, though, integrable special cases of spinning top motion. One of them is the Lagrange top, a rotationally symmetric body with the fixed point on the symmetry axis. Then the third component of the vector of angular momentum in the body frame (a frame firmly attached to the body and the origin at the fixed point) is a third integral of motion, additional to the energy and third component of the angular momentum in the rest frame (a frame constant in time, so that the gravity is parallel to the third axis), which are always constant. This assures its complete integrability. But only recently Prof. A. I. Bobenko and Prof. Yu. B. Suris found an integrable discretization for the Lagrange tops path. In [BS00], they used the following

Theorem 1.1 (Kirchhoffs kinetic analogy)**.** *The paths of Lagrange top body frames are in a one to one correspondence to the frames of elastic curves.*

to derive an integrability preserving discretization, which will be called the *Bobenko-Suris discretization* from now on. Elastic curves are thereby curves that minimize their bending energy for fixed length, boundary points and velocity vectors at the boundary.

Comparison of the *Bobenko-Suris discretization* to numerical ones In the present work now a qualitative assessment of this discretization is done. This is achieved with an actual calculation and visualization in a *Java*^{TM} application called *Top Visualization*. To have a comparison to existing discretizations, the tops paths are calculated in essentially three different ways for identical initial data: once with a very small discretization step length parameter ε to have a result close to the "real", the continuous one; second with a known numerical discretization with a bigger ε, i. e. to have a really discrete motion; and third with the integrable discretization with again a big ε.

As result, two things turn out clearly. First the *Bobenko-Suris discretization* has a flaw. Denoting m the vector of angular momentum, a the vector pointing to the center of mass and g the gravity vector, all in the rest frame, the *Bobenko-Suris* discretization does *not* preserve the energy of the Lagrange top

$$H = \frac{1}{2}\langle m, m\rangle + \langle a, p\rangle \,.$$

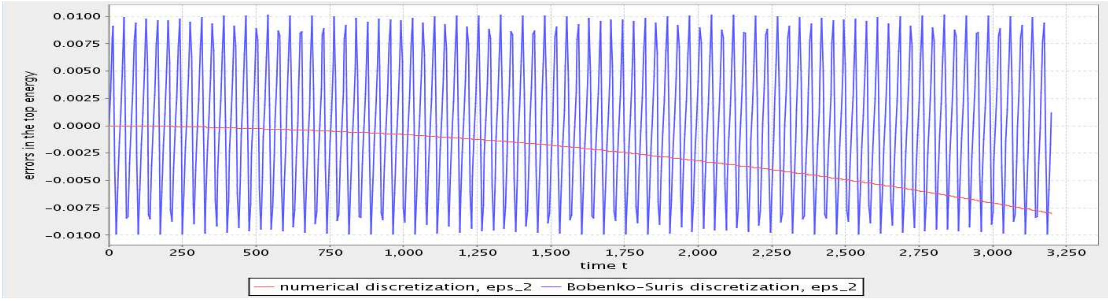

Figure 1.1: Errors in the energy for the numerical and the *Bobenko-Suris discretization*. In the beginning the numerical error is small, but it propagates somewhat quadratic so it surpasses the oscillating error in the integrable case eventually.

Instead it preserves the term

$$H_\varepsilon = \frac{1}{2}\langle m, m\rangle + \langle a, p\rangle + \frac{\varepsilon}{2}\langle a \times m, p\rangle .$$

The additional term causes a quite high deviation from the real energy, which in turn results in an error in the tops body frame. So the calculated path is a different one from the continuous, which shows itself already after short time periods. Nontheless, the second observation is that, though the numerical discretization is always better in the beginning, eventually its errors will exceed the ones of the integrable discretization. In figure 1.1 it can be seen that the numerical error propagation is somewhat quadratic, whereas the error in the *Bobenko-Suris discretization* oscillates.

Visualizations Once the program was written to find these results, it lent itself to enhance its functionality to other interesting visualizations. There are now, for instance, two more integrable cases of rigid body motion visualized, namely the *Kowalewski* and the *Goryachev-Chaplygin* tops.[1]

In order to visualize them, the numerical calculation of the top motion was implemented for general spinning tops. For that it proved useful to find a form of the Kirchhoff equations in the rest frame, which reads

$$\begin{aligned} \omega' &= A^{-1}(A\omega \times \omega + \mathcal{M} \cdot p \times a) \qquad \text{where} \\ A &= I_N \cdot NN^t + I_B \cdot BB^t + I_T \cdot TT^t . \end{aligned}$$

Thereby ω is the vector of angular velocity, $\mathcal{M}$ the total mass, (N, B, T) the body frame and I_N, I_B, I_T the principal moments of inertia of the body. The gravity vector is then the (constant) third rest frame vector and the path of the body frame can be reproduced from ω.

Furthermore there is a visualization of Kirchhoffs kinetic analogy 1.1 and also of its generalization to elastic rods, i. e. when including a twist energy as penality for torsion of the rod. Elastic curves then are isotropic elastic rods, which have a symmetric cross section (e. g. round or square). The generalization is then that elastic rods in general correspond to spinning tops with the fixed point on one of its principal axes. Now, there are Kowalewski and Goryachev-Chaplygin tops with that property, so there exists a corresponding elastic rod. These corresponding objects are visualized together in the *Top Visualization*

[1]The last integrable case is the Euler top, having its fixed point at the center of mass. But this one is already well known and not very interesting to visualize.

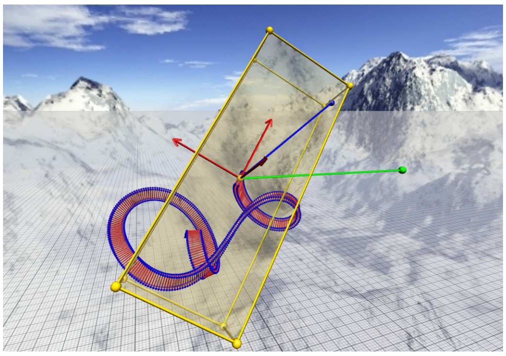

(a) A Goryachev-Chaplygin top with its corresponding (anisotropic) elastic rod.

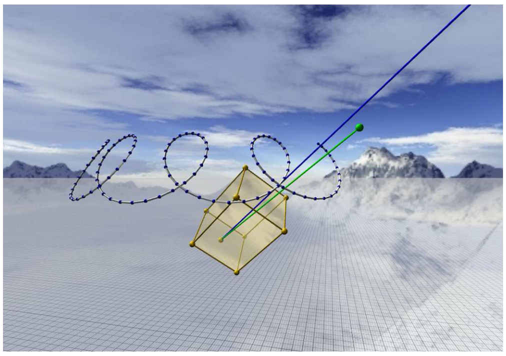

(b) A Lagrange top with its precession and nutation visualized in the so called *apex trace*.

Figure 1.2: Example visualizations.

program, and also the isotropic elastic rods corresponding to Lagrange tops can be studied. For an example of a Goryachev-Chaplygin top with its corresponding elastic rod see figure 1.2(a).

Studying spinning top motions is not limited to special cases either in the *Top Visualization* program. One starts with a certain quader, but can edit it to arbitrary quader with arbitrary fixed points; and since the motion of spinning tops is determined by its fixed point and its principal moment of inertia, the motion of the body frame of every spinning top can be seen.

Finally there is a visualization of the typical 2-periodic behaviour of the symmetry axis of Lagrange tops, the so called precession and nutation. Therefore the point of intersection of the symmetry axis with a sphere around the bodys fixed point is drawn and connected at every motion step. This so called *apex trace* can be seen at an example in figure 1.2(b).

The thesis is organized as follows:

In chapter 2 the basics about spinning tops in general and the Lagrange top in special are recalled. In examples these are applied to quader, which are the special case of spinning tops used in the *Top Visualization* program.

Chapter 3 is devoted to the continuous dynamics of spinning tops. There basic variational principles and the matrix groups $su(2)$ and $SU(2)$ are recalled, with whose help the formulation of Kirchhoffs equations in the rest frame is then derived. Further the derivation of Kirchhoffs kinetic analogy and its generalization is given at the end of this chapter.

Chapter 4 is devoted to the different discretizations of the paths of spinning tops. First the basic facts on the numerical discretization used in the *Top Visualization* program are given, then the integrable discretization found by Prof. A. I. Bobenko and Prof. Yu. B. Suris is presented. For its derivation see the original paper [BS00].

The complete description, functionality and features of the *Top Visualization* program are given in chapter 5. The program can be found on the CD attached to the back cover, under http://www.math.tu-berlin.de/~bodack or as webstart application under http://www.math.tu-berlin.de/geometrie/ps/software.shtml and used to compare the discretizations oneself.

The results of an exemplary comparison are given in chapter 6. Further there are the results of two other, non-repeatable experiments given in chapter 6 which give additional insight into the properties of the *Bobenko-Suris discretization*.

Chapter 2

The Spinning Top

2.1 Definition

Definition. A *rigid body* is a set of points in euclidean space which move in time and preserve their distance, i. e.

$$\|x(t) - y(t)\| = const \qquad \forall t \tag{2.1}$$

where t is the time and x and y two points of the body moving with t. Or more precisely, $x, y : T \to \mathbb{R}^3$, $t \mapsto x(t)$, $t \mapsto y(t)$, $t \in T$ are continuous functions.

Definition. A *fixed point* is a point in euclidean space which stays constant in time.

Definition. A *spinning top* is a rigid body in a homogeneous[1] gravitational field that moves around a fixed point, i. e.

$$\|x(t) - O\| = const \qquad \forall t,\ x,\ y \tag{2.2}$$

where O is the fixed point and x a point of the body.

Example. The spinning top used in the *Top Visualization* program desribed in chapter 5 is a homogeneous quader, the fixed point is at the origin and (in most of the examined cases) at the center of one of the quader faces. See figure 2.1.

2.2 Motion, vector of angular velocity, vector of angular momentum

Definition. The *vector of angular velocity* at time t of a rigid body rotating around the origin is the vector $\omega(t) \in \mathbb{R}^3$ that satisfies

$$\dot{x}(t) = \omega(t) \times x(t) \tag{2.3}$$

for all points of the body.

Remark. The general case of motion of a rigid body can be described by a displacement of the center of mass of the body plus a rotation around it.

The spinning top motion is limited to a rotation around the fixed point and is therefore determined by three independent variables. Knowledge of the instantaneous rotation axis and the rotation speed therefore

[1]constant

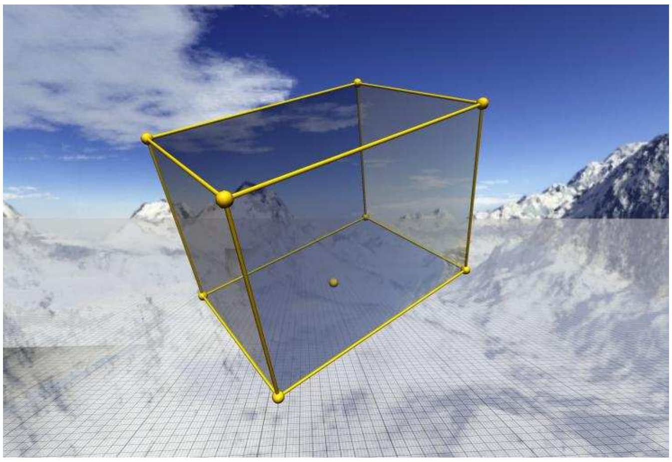

Figure 2.1: Quader with fixed point at the center of one of its faces.

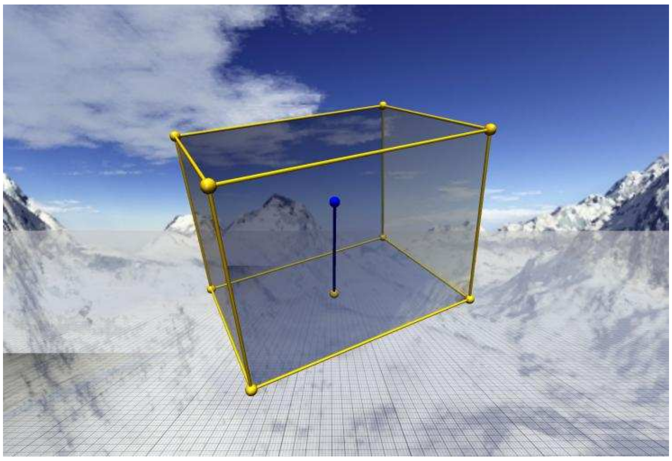

Figure 2.2: Quader with its vector of angular velocity.

completely suffices. It can be unified in the *vector of angular velocity*, which points in the direction of the rotation axis and has the length of the rotation speed. It is usually denoted with ω. The direction of the vector can be determined by the *right hand rule*[2].

Example. The vector of angular velocity in the *Top Visualization* program is blue. See figure 2.2.

Definition. The *vector of angular momentum* $m(t)$ of a point $x(t)$ with mass $\mathcal{M}$ is defined by

$$m(t) = x(t) \times \mathcal{M}\dot{x}(t),$$

i. e. the cross product of the point with its *linear* momentum.

For a body within the area V with mass density function $\rho(q)$ the vector of angular momentum is

$$m(t) := \int_V q(t) \times \rho(q)\, \dot{q}(t)\, \mathrm{d}q.$$

[2] Point your right thumb up, curl the other fingers, they show the direction of the rotation.

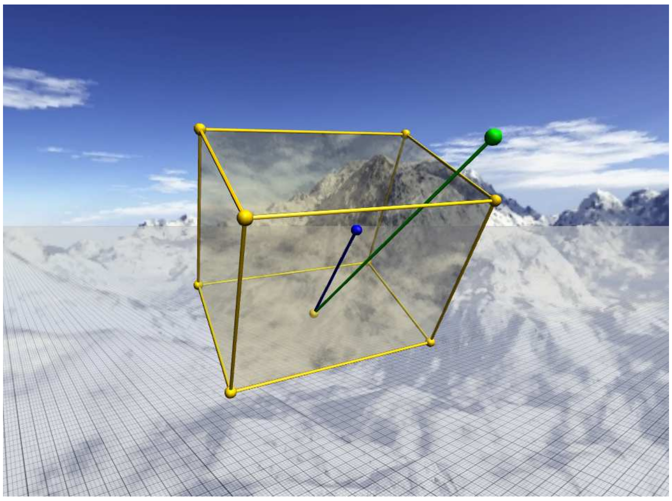

Figure 2.3: Quader with its vector of angular velocity (blue) and vector of angular momentum (green).

Example. The vector of angular momentum in the *Top Visualization* program is green. See figure 2.3.

2.3 Moments of inertia, inertia tensor, body frame

2.3.1 General

Definition. The *moment of inertia* of a body wrt an axis l is

$$I_l := \int_V \rho(q)\, r_l^2(q)\, \mathrm{d}q \tag{2.4}$$

where ρ is the density function of the body, $V \subset \mathbb{R}^3$ a region containing the body and $r_l(q)$ the distance of q to the l axis.[3]

Remark. Physically the moment of inertia is for a rotational acceleration what the mass is for a rectilinear one. It is a measure for the resistance against accelerating the body around the axis l.

There is a connection between the *vector of angular velocity*, the *vector of angular momentum* and the *moments of inertia* of a body, the so called *inertia tensor*. It will prove useful to unite all *moments of inertia* of a body rotating around a fixed point and yield the *body frame* of the body, with whose help the calculation of the body motion will be much simplified.

Definition. The *inertia tensor* of a rigid body is that linear mapping J which maps the body's *vector of angular velocity* to its *vector of angular momentum*, i. e.

$$m = J\omega. \tag{2.5}$$

Remark (Existence and calculation). If the body is contained in the region V and has density function ρ,

[3] For a body containing only a finite number of points the integral changes to a sum.

then in shortened notation:

$$\begin{aligned}
m &= \int\limits_V q \times \rho(q)\, \dot{q}\, \mathrm{d}q \\
&\overset{def}{=} \int\limits_V \rho(q) \cdot q \times (\omega \times q)\, \mathrm{d}q \\
&\overset{(2.6)}{=} \int\limits_V \rho(q) \cdot \Big(\omega \left\langle q, q \right\rangle - q \left\langle q, \omega \right\rangle \Big)\, \mathrm{d}q \\
&\overset{(2.7)}{=} \int\limits_V \rho(q) \cdot \Big(\left\langle q, q \right\rangle E(3) - q \cdot q^t \Big)\, \mathrm{d}q \cdot \omega
\end{aligned}$$

Thereby $E(3)$ denotes the unit 3×3 matrix. Further the *bac-cab* rule

$$a \times (b \times c) = b \left\langle a, c \right\rangle - c \left\langle a, b \right\rangle \tag{2.6}$$

and

$$\left\langle a, b \right\rangle a = (a \cdot a^t) \cdot b \tag{2.7}$$

were used. Hence

$$J = \int\limits_V \rho(q) \cdot \Big(\left\langle q, q \right\rangle E(3) - q \cdot q^t \Big)\, \mathrm{d}q.$$

The latter integral depends on the origin of the chosen coordinate system (the fixed point), so J does too.

Now for a given body the vector of angular momentum can be calculated from the vector of angular velocity and vice versa. The connection between the inertia tensor and the moments of inertia clarifies the following

Lemma 2.1. *Let J be the inertia tensor of a body wrt the fixed point (the origin) and l an axis through the origin, then the moment of inertia of the body wrt l is*

$$I_l = \vec{l}^t \cdot J \cdot \vec{l} = \left\langle \vec{l}, J\vec{l} \right\rangle \tag{2.8}$$

where $\vec{l}$ is a unit vector spanning l.

Proof.

$$\begin{aligned}
\left\langle \vec{l}, J\vec{l} \right\rangle &= \left\langle \vec{l}, \int\limits_V \rho(q) \cdot \Big(\left\langle q, q \right\rangle E(3) - q \cdot q^t \Big)\, \mathrm{d}q \cdot \vec{l} \right\rangle \\
&= \int\limits_V \rho(q) \left\langle \vec{l}, \Big(\left\langle q, q \right\rangle E(3) - q \cdot q^t \Big) \cdot \vec{l} \right\rangle \mathrm{d}q \\
&= \int\limits_V \rho(q) \Big(\left\langle q, q \right\rangle \left\langle \vec{l}, \vec{l} \right\rangle - \vec{l}^t \cdot q \cdot q^t \cdot \vec{l} \Big)\, \mathrm{d}q \\
&= \int\limits_V \rho(q) \Big(\left\langle q, q \right\rangle - \left\langle \vec{l}, q \right\rangle \left\langle q, \vec{l} \right\rangle \Big)\, \mathrm{d}q
\end{aligned}$$

Since r_l, the distance of the point q to the axis l, satisfies

$$r_l^{\,2}(q) = \left\langle q, q \right\rangle - \left\langle q, \vec{l} \right\rangle^2 \tag{2.9}$$

(Pythagorean theorem) we get

$$\left\langle \vec{l}, J\vec{l} \right\rangle = \int_V \rho(q) \cdot {r_l}^2(q)\, \mathrm{d}q = I_l$$

□

Another interesting property of the inertia tensor gives the following

Lemma 2.2. *The inertia tensor J is symmetric.*

Proof. It is to show that for arbitrary vectors a and b it holds

$$\langle a, Jb \rangle = \langle Ja, b \rangle \, .$$

Now

$$\begin{aligned} \langle a, Jb \rangle &= \left\langle a, \int_V \rho(q) \Big(\langle q, q \rangle \, E(3) - q \cdot q^t \Big) \, \mathrm{d}q \cdot b \right\rangle \\ &= \left\langle a, \int_V \rho(q) \Big(\langle q, q \rangle \, b - q \cdot q^t \cdot b \Big) \, \mathrm{d}q \right\rangle \\ &= \int_V \rho(q) \left\langle a, \Big(\langle q, q \rangle \, b - q \, \langle q, b \rangle \Big) \right\rangle \, \mathrm{d}q \\ &\overset{(2.6)}{=} \int_V \rho(q) \, \langle a, q \times (b \times q) \rangle \, \mathrm{d}q \\ &= \int_V \rho(q) \, \langle b \times q, a \times q \rangle \, \mathrm{d}q, \end{aligned} \tag{2.10}$$

where the last step is the circular symmetry of the triple scalar product (the determinant).
The fact that the last expression is symmetric wrt a and b completes the proof. □

As a first conclusion, one can calculate the kinetic energy of the body with the help of the inertia tensor.

Corollary 2.3. *Let a rigid body be fixed at the origin, J be its inertia tensor at the origin and ω its vector of angular velocity, then the kinetic energy of the body is*

$$T = \frac{1}{2} \langle \omega, J\omega \rangle \, . \tag{2.11}$$

Proof. Using equation (2.10) one gets

$$\begin{aligned} \frac{1}{2} \langle \omega, J\omega \rangle &= \frac{1}{2} \int_V \rho(q) \, \langle \omega \times q, \omega \times q \rangle \, \mathrm{d}q \\ &= \frac{1}{2} \int_V \rho(q) \, \langle \dot{q}, \dot{q} \rangle \, \mathrm{d}q \end{aligned}$$

and the last expression is mass times velocity squared integrated over the body, hence the kinetic energy.
□

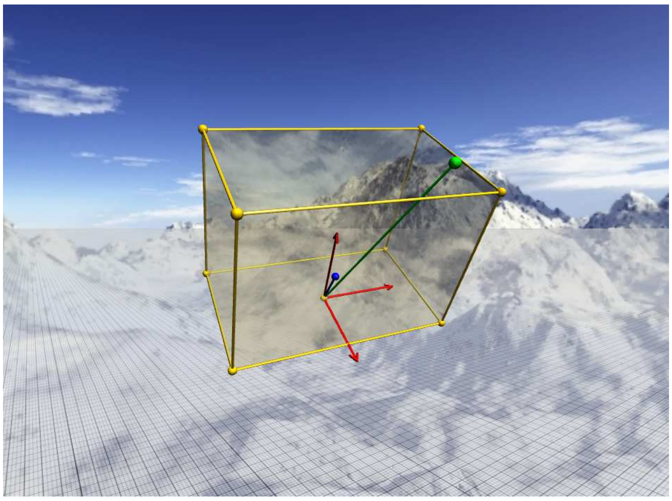

Figure 2.4: The bodyframe of a quader.

Further the symmetry of the inertia tensor implies that there exists an orthogonal frame of Eigenvectors of J. It is called:

Definition. The *body frame* of a rigid body is a positively oriented orthonormal frame of Eigenvectors of the inertia tensor of the body at the fixed point. The axes spanned by the fixed point and the Eigenvectors are called *principal axes*, the corresponding moments of inertia *principal moments of inertia*.

In the present work the (vectors of the) body frame will be denoted by

$$(N, B, T)$$

and for distinction a stationary frame with the same origin and orientation will be called a *rest frame* and denoted by

$$(e_1, e_2, e_3).$$

Example. For the body frame of a quader with fixed point at the center of one of its faces see figure 2.4. The red arrows are the basis vectors N, B and T of the body frame. Note that they are parallel to the quaders edges. The derivation of this result will follow later this section.

2.3.2 Application to a quader, notations

In this subsection proper notations for handling a quader with unit density and the fixed point at the center of one of its faces are introduced, with which the mass, moments of inertia and inertia tensor can be expressed more easily. Alongside some theory that helps with the necessary calculations is provided.

First, the principal axes and hence the body frame of a quader wrt its center of mass a are calculated. Recall that, if the fixed point is at the origin, the inertia tensor is

$$J_a = \int_V \rho(q) \Big(\langle q, q \rangle \, E(3) - q \cdot q^t \Big) \, \mathrm{d}q,$$

where q is the position vector wrt a coordinate system with a as origin. Unit density means $\rho \equiv 1$. A reasonable choice of a basis is a positively oriented orthonormal basis with vectors parallel to the quader

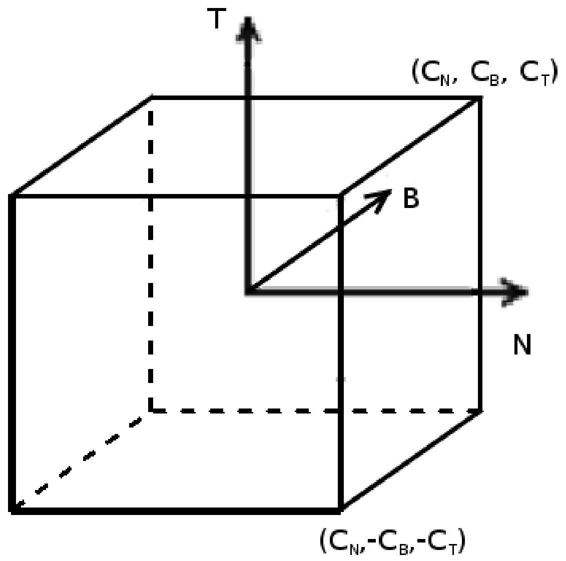

Figure 2.5: Quader coordinates in the body frame wrt the center of mass.

axes, see figure 2.5. This frame will turn out to be the body frame, so it can be denoted by (N, B, T). Then the vertices of the quader are determined by a set of positive numbers $(C_N, C_B, C_T) \in \mathbb{R}^3_+$, see again figure 2.5.

In these coordinates, the rotation from the rest to the body frame has Jacobian 1, it holds

$$\begin{aligned} J_a &= \int\limits_{-C_N}^{C_N} \int\limits_{-C_B}^{C_B} \int\limits_{-C_T}^{C_T} \langle q, q \rangle \, E(3) - q \cdot q^t \, \mathrm{d}q_0 \, \mathrm{d}q_1 \, \mathrm{d}q_2 \\ &= \int\limits_{-C_N}^{C_N} \int\limits_{-C_B}^{C_B} \int\limits_{-C_T}^{C_T} \begin{pmatrix} q_1^2 + q_2^2 & -q_0 q_1 & -q_0 q_2 \\ -q_0 q_1 & q_0^2 + q_2^2 & -q_1 q_2 \\ -q_0 q_2 & -q_1 q_2 & q_0^2 + q_1^2 \end{pmatrix} \mathrm{d}q_0 \, \mathrm{d}q_1 \, \mathrm{d}q_2 \end{aligned}$$

Evaluating for $i \neq j \neq k \neq i$

$$\begin{aligned}
\int_{-C_N}^{C_N}\int_{-C_B}^{C_B}\int_{-C_T}^{C_T}(q_i^2+q_j^2)\,\mathrm{d}q_0\mathrm{d}q_1\mathrm{d}q_2 &= 8\cdot\int_0^{C_N}\int_0^{C_B}\int_0^{C_T}(q_i^2+q_j^2)\,\mathrm{d}q_0\mathrm{d}q_1\mathrm{d}q_2\\
&= 8\cdot C_k\int_0^{C_j}\Big[\frac{1}{3}q_i^3+q_iq_j^2\Big]_{q_i=0}^{C_i}\mathrm{d}q_j\\
&= 8\cdot C_k\cdot C_i\int_0^{C_j}(\frac{C_i^2}{3}+q_j^2)\,\mathrm{d}q_j\\
&= 8\cdot C_k\cdot C_i\Big[\frac{C_i^2}{3}q_j+\frac{1}{3}q_j^3\Big]_{q_j=0}^{C_j}\\
&= \frac{8\cdot C_N\cdot C_B\cdot C_T}{3}(C_i^2+C_j^2)
\end{aligned}$$

and

$$\begin{aligned}
\int_{-C_N}^{C_N}\int_{-C_B}^{C_B}\int_{-C_T}^{C_T}(-q_iq_j)\,\mathrm{d}q_0\mathrm{d}q_1\mathrm{d}q_2 &= 2\cdot C_k\int_{-C_j}^{C_j}\Big[-\frac{1}{2}q_i^2q_j\Big]_{q_i=-C_i}^{C_i}\mathrm{d}q_0\,\mathrm{d}q_j\\
&= 2\cdot C_k\int_{-C_j}^{C_j}\Big(-\frac{1}{2}C_i^2q_j+\frac{1}{2}C_i^2q_j\Big)\,\mathrm{d}q_0\,\mathrm{d}q_j\\
&= 0
\end{aligned}$$

gives

$$J_a=\frac{\mathcal{M}}{3}\begin{pmatrix}{C_B}^2+{C_T}^2 & 0 & 0\\ 0 & {C_N}^2+{C_T}^2 & 0\\ 0 & 0 & {C_N}^2+{C_B}^2\end{pmatrix}.$$

The fact that J_a is already diagonal in the frame (N,B,T) shows that this is indeed the body frame wrt the center of mass. The mass of the quader $\mathcal{M}=8\cdot C_N\cdot C_B\cdot C_T$ can be immediately seen from figure 2.5, since it has unit density.

An example for such a body frame of a quader visualized in the *Top Visualization* program can be seen in figure 2.6.

Now a summary of notations:

Definition (Notations)**.** The coordinates of the vertices of the quader in the body frame are determined by a set of positive numbers $(C_N,C_B,C_T)\in\mathbb{R}_+^3$. This set will be called the *coordinates of the quader* or *quader coordinates*. See figure 2.5. Coordinates of vectors wrt the restframe will get small letters, wrt the bodyframe big ones, e. g.

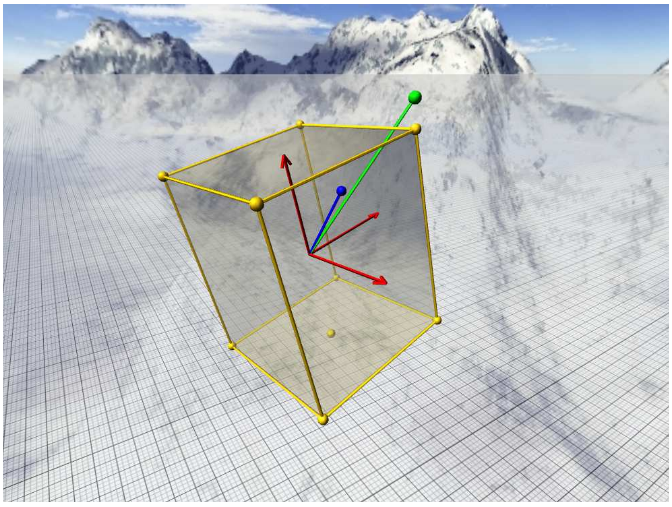

Figure 2.6: Body frame wrt the center of mass of a quader.

(N, B, T)	the body frame
(e_1, e_2, e_3)	the rest frame
q	radius vector of a point in the rest frame
Q	radius vector of a point in the body frame
ω	vector of angular velocity in the rest frame
Ω	vector of angular velocity in the body frame
m	vector of angular momentum in the rest frame
M	vector of angular momentum in the body frame
p	gravity vector in the rest frame (p is constant)
P	gravity vector in the body frame
$\mathcal{M}$	the mass of the body
I_i	(principal) moment of inertia wrt the axis spanned by e_i

The results so far are useful for rotations around the center of mass. For arbitrary fixed points one needs the inertia tensor at an arbitrary point. But this is easily calculated with the following two statements.

Theorem 2.4 (Parallel axes theorem or Huygens-Steiners theorem)**.** *Let l be an axis passing through the center of mass a of a body and s an axis parallel to l, then the moments of inertia of the body wrt those axes satisfy*

$$I_s = I_l + \mathcal{M} \cdot d^2 \tag{2.12}$$

where d is the distance between the l and s axes, see figure 2.7(a).

Proof. By the law of cosines

$$r_s^2(q) = d^2 + r_l^2(q) - 2d\, r_l(q) \cos\phi$$

where $r_l(q)$ is the distance of q to l, $r_s(q)$ the distance of q to s and ϕ the angle like in figure 2.7(b).

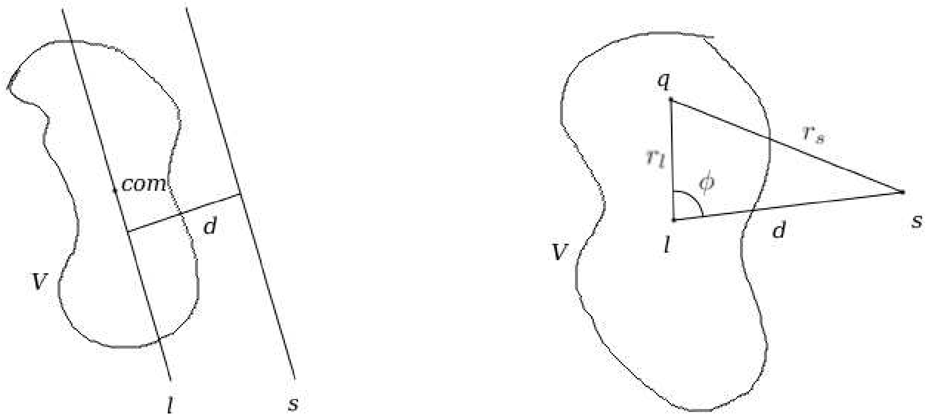

(a) Viewed in a plane spanned by the axes. (b) Viewed in a plane perpendicular to the axes.

Figure 2.7: Body with two parallel rotation axes.

Hence

$$\begin{aligned} I_s &= \int\limits_V \rho(q)\, r_s^2(q)\,\mathrm{d}q \\ &= \int\limits_V \rho(q)\, d^2\,\mathrm{d}q + \int\limits_V \rho(q)\, r_l^2(q)\,\mathrm{d}q - 2\int\limits_V \rho(q)\, d\, r_l(q)\cos\phi\,\mathrm{d}q \\ &= d^2 \int\limits_V \rho(q)\,\mathrm{d}q + \int\limits_V \rho(q)\, r_l^2(q)\,\mathrm{d}q - 2d\int\limits_V \rho(q)\, r_l(q)\cos\phi\,\mathrm{d}q \\ &= \mathcal{M}\cdot d^2 + I_l - 2d\int_V \rho(q)\, r_l(q)\cos\phi\,\mathrm{d}q \end{aligned}$$

So it suffices to show that

$$\int\limits_V \rho(q)\, r_l(q)\cos\phi\,\mathrm{d}q = 0 \tag{2.13}$$

By definition of the center of mass,

$$a = \frac{1}{\mathcal{M}} \int\limits_V \rho(q)\, q\,\mathrm{d}q.$$

Choosing a coordinate system with the origin at the center of mass a and l pointing in z-direction, further expressing q in cylindrical coordinates, one gets

$$0 = \int\limits_V \rho(q) \begin{pmatrix} r_l\cos\phi \\ r_l\sin\phi \\ z \end{pmatrix} \mathrm{d}q$$

whose first coordinate is the desired equation (2.13). □

Corollary 2.5. *Let a be the center of mass of a rigid body and J_a its inertia tensor, p another point displaced from a by the vector $\vec{r}$ and J_p the body's inertia tensor wrt p. Then*

$$J_p = J_a + \mathcal{M}\Big(\langle\vec{r},\vec{r}\rangle\, E(3) - \vec{r}\cdot\vec{r}^{\,t}\Big) \tag{2.14}$$

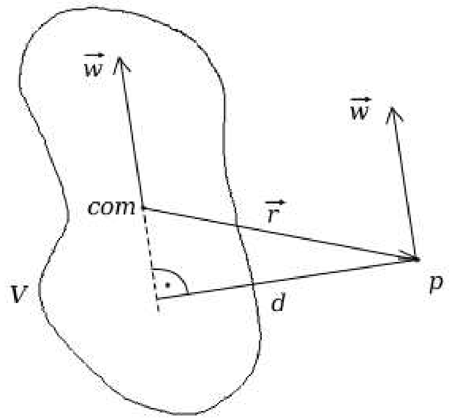

Figure 2.8: Inertia tensor wrt the center of mass and a second point p.

where $E(3)$ is the 3x3 unit matrix. See figure 2.8.

Proof. The moment of inertia of the body wrt the axis through the center of mass a pointing in the direction of a unit vector $\vec{w}$ is

$$I_{\vec{w},a} = \langle \vec{w}, J_a \vec{w} \rangle \, .$$

By the parallel axes theorem,

$$I_{\vec{w},p} = I_{\vec{w},a} + \mathcal{M} \cdot d^2 .$$

Now,

$$d^2 = \langle \vec{r}, \vec{r} \rangle - \langle \vec{r}, \vec{w} \rangle^2$$

and hence

$$\begin{aligned} \langle \vec{w}, J_p \vec{w} \rangle &= \langle \vec{w}, J_a \vec{w} \rangle + \mathcal{M} \Big(\langle \vec{r}, \vec{r} \rangle - \langle \vec{r}, \vec{w} \rangle \langle \vec{r}, \vec{w} \rangle \Big) \\ &= \langle \vec{w}, J_a \vec{w} \rangle + \mathcal{M} \Big(\langle \vec{r}, \vec{r} \rangle \langle \vec{w}, \vec{w} \rangle - \langle \vec{w}, \langle \vec{r}, \vec{w} \rangle \vec{r} \rangle \Big) \\ &= \langle \vec{w}, J_a \vec{w} \rangle + \mathcal{M} \Big(\langle \vec{w}, \langle \vec{r}, \vec{r} \rangle \vec{w} \rangle - \big\langle \vec{w}, \vec{r} \cdot \vec{r}^t \vec{w} \big\rangle \Big) \\ &= \Big\langle \vec{w}, \Big[J_a + \mathcal{M} \Big(\langle \vec{r}, \vec{r} \rangle E(3) - \vec{r} \cdot \vec{r}^t \Big) \Big] \vec{w} \Big\rangle \end{aligned}$$

□

Corollary 2.6. *For a quader with quader coordinates (C_N, C_B, C_T) in body frame (N, B, T) attached to the center of mass, the point with coordinates $(0, 0, -C_T)$ lies on the center of one of the quader faces. The inertia tensor of the quader wrt this point is*

$$J = \frac{\mathcal{M}}{3} \begin{pmatrix} {C_B}^2 + (2C_T)^2 & 0 & 0 \\ 0 & {C_N}^2 + (2C_T)^2 & 0 \\ 0 & 0 & {C_N}^2 + {C_B}^2 \end{pmatrix} .$$

Proof. It is clear that the point lies at the center of a quader face. For the inertia tensor one gets with the preceding corollary

$$\begin{aligned} J &= J_a + \mathcal{M}\Big(\langle \vec{r}, \vec{r} \rangle \, E(3) - \vec{r} \cdot \vec{r}^t \Big) \\ &= \frac{\mathcal{M}}{3} \begin{pmatrix} {C_B}^2 + {C_T}^2 & 0 & 0 \\ 0 & {C_N}^2 + {C_T}^2 & 0 \\ 0 & 0 & {C_N}^2 + {C_B}^2 \end{pmatrix} + \mathcal{M}\left(C_T^2 \cdot E(3) - \begin{pmatrix} 0 & 0 & 0 \\ 0 & 0 & 0 \\ 0 & 0 & C_T^2 \end{pmatrix} \right) \\ &= \frac{\mathcal{M}}{3} \begin{pmatrix} {C_B}^2 + (2C_T)^2 & 0 & 0 \\ 0 & {C_N}^2 + (2C_T)^2 & 0 \\ 0 & 0 & {C_N}^2 + {C_B}^2 \end{pmatrix} \end{aligned}$$

□

Since J stayed diagonal, the body frame stays the same, but is just attached to the new fixed point $(0, 0, -C_T)$. See again figure 2.4. In the *Top Visualization* program this point is the fixed point and this inertia tensor the one relevant for the body motion.

2.4 The Lagrange top

Definition. A *Lagrange top* is a spinning top which is symmetric wrt a rotation[4] around an axis through the fixed point.

Remark. The rotational symmetry implies that the center of mass of the body lies on the symmetry axis. Would it lie elsewhere it would move during the rotation and the body could not be the same as before.

The Lagrange top is an interesting case of rigid body motion since it is integrable. More about that will follow in the next chapter.

Example. A homogeneous[5] quader with coordinates (C_N, C_N, C_T) is mapped to itself by a rotation by the angle $\pi/2$ around T, the third axis of the body frame. Hence, if the fixed point lies on that axis, the quader is a Lagrange top. See figure 2.9.

The Lagrange top visualized in the *Top Visualization* program has the fixed point at $-C_T \cdot T$ which is $(0, 0, -C_T)$ in body frame coordinates.

[4] The body is mapped to itself by a rotation by $2\pi/n$ for an $n > 2$.

[5] Constant density function.

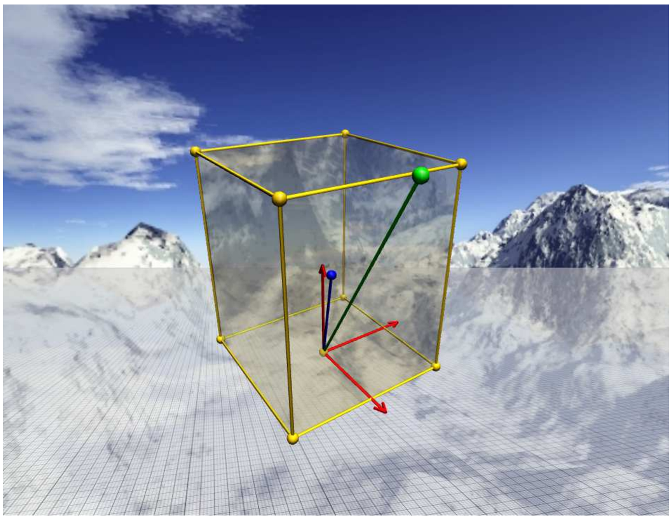

Figure 2.9: A Lagrange top.

Chapter 3

Dynamics

In this section the (continuous) equations of motion of a spinning top in the rest frame[1] are derived. Therefore the necessary variational principals and the energy of the spinning top are recalled. For a simplification of calculations an isomorphism between $\mathbb{R}^3$ and the matrix group $su(2)$ as well as the motion group $SO(3)$ and $SU(2)$ are introduced.

Further the analogies between Lagrange tops and elastic curves (Kirchhoffs analogy) as well as spinning tops and elastic rods are presented. The former served as the guiding idea for finding an integrable discretization of the Lagrange top, as described in [BS00] and implemented in the *Top Visualization* program.

3.1 Variational principals

Definition. Let

$$\begin{array}{rcl} L:\ \mathbb{R}^n \times \mathbb{R}^n \times [t_0, t_1] & \longrightarrow & \mathbb{R} \\ (p, q, t) & \longmapsto & L(p, q, t) \end{array}$$

be a twice differentiable functional. Then a twice differentiable curve

$$f:\ [a, b] \longmapsto \mathbb{R}^n$$

is called an *extremal of the functional*

$$S(f) = \int_{t_0}^{t_1} L(f(t), f'(t), t)\,\mathrm{d}t$$

if it minimizes S over the set of all twice differentiable funtions on $[t_0, t_1]$ with the same values as f at t_0 and t_1.

Theorem 3.1 (Hamilton's principal of least action)**.** *Motions of mechanical systems*[2] *coincide with extremals of the functional*

$$S(f) = \int_{t_0}^{t_1} L(f(t), f'(t), t)\,\mathrm{d}t,$$

[1]The equations of motion in the body frame are the well known Kirchhoff equations, but a rest frame formulation will prove useful for finding a numerical solution.

[2]Systems in which Newtons equations of motion hold.

where

$$L = T - U$$

is the difference between the kinetic and the potential energy, the so called Lagrange function *or* Lagrangian.

Proof. Omitted. See e. g. [Arn]. □

Definition. A *variation* of a curve $f : [t_0, t_1] \to \mathbb{R}^n, t \mapsto f(t)$ is a twice differentiable function

$$\begin{array}{rcl} f_\varepsilon : [t_0, t_1] \times [-\epsilon, \epsilon] & \longrightarrow & \mathbb{R}^n \\ (t, \varepsilon) & \longmapsto & f_\varepsilon(t, \varepsilon) \end{array}$$

that satisfies

$$f_\varepsilon(t, 0) = f(t) \quad \forall t \in [t_0, t_1],$$

$$f_\varepsilon(t_0, \varepsilon) = f(t_0) \quad \forall \varepsilon \in [-\epsilon, \epsilon]$$

and

$$f_\varepsilon(t_1, \varepsilon) = f(t_1) \quad \forall \varepsilon \in [-\epsilon, \epsilon].$$

Lemma 3.2. *An extremal $f(t)$ of a functional $S(f)$ satisfies*

$$0 = \frac{\mathrm{d}}{\mathrm{d}\varepsilon} \int_{t_0}^{t_1} L(f_\varepsilon(t, \varepsilon), f'_\varepsilon(t, \varepsilon), t) \, \mathrm{d}t \bigg|_{\varepsilon=0}$$

for all variations f_ε of f.

Proof. Omitted. See e. g. [Arn]. □

Lemma 3.3 (Fundamental lemma of calculus of variations)**.** *If a continuous function $f : [t_0, t_1] \to \mathbb{R}$ satisfies*

$$\int_{t_0}^{t_1} f(t) h(t) \, \mathrm{d}t = 0$$

for all continuous function $h(t)$ with $h(t_0) = h(t_1) = 0$, then

$$f(t) \equiv 0.$$

Proof. Omitted. See e. g. [Arn]. □

Remark. With the stated principals one can already find the equations of motion of a spinning top. The function f is the position of the top at time t, i. e. the rotation from the rest frame to the body frame. But dealing with rotations is much more convenient in the Lie group $SU(2)$ and its Lie algebra $su(2)$ compared to the rotation group $SO(3)$ and $so(3)$. The isomorphism between them is introduced in short in the next chapter, for more details see [B06].

3.2 Rotation in $\mathbb{R}^3$, $su(2)$ and $SU(2)$

3.2.1 The vector space $su(2)$

The set of skew symmetric complex two by two matrices with trace zero

$$su(2) := \{A \in gl(2,\mathbb{C}), A^* = -A, tr(A) =)\}$$

is a vector space and

$$e_1 = \frac{1}{2}\begin{pmatrix} 0 & -i \\ -i & 0 \end{pmatrix}, e_2 = \frac{1}{2}\begin{pmatrix} 0 & -1 \\ 1 & 0 \end{pmatrix}, e_3 = \frac{1}{2}\begin{pmatrix} -i & 0 \\ 0 & i \end{pmatrix}$$

a basis[3] of $su(2)$, since

$$A = \begin{pmatrix} a & b \\ c & d \end{pmatrix} \quad a,b,c,d \in \mathbb{C}$$
$$\Rightarrow A^* = -A \Leftrightarrow \bar{a} = -a,\ \bar{d} = -d,\ \bar{b} = -c \text{ and } \bar{c} = -b$$
$$\Leftrightarrow A = \begin{pmatrix} i\alpha & b \\ -\bar{b} & i\delta \end{pmatrix}, \quad \alpha, \delta \in \mathbb{R}$$
$$tr(A) = 0 \Leftrightarrow \alpha = -\delta$$
$$\Rightarrow A \in su(2) \Leftrightarrow A = \begin{pmatrix} i\alpha & \beta + i\gamma \\ -\beta + i\gamma & -i\alpha \end{pmatrix} = -2\gamma e_1 - 2\beta e_2 - 2\alpha e_3 \quad \alpha, \beta, \gamma \in \mathbb{R}.$$

This gives an isomorphism between $\mathbb{R}^3$ and $su(2)$. I. e. a vector $x = (x_1, x_2, x_3)$ is identified with the matrix $\hat{x} = \frac{1}{2}\begin{pmatrix} -ix_3 & -x_2 - ix_1 \\ x_2 - ix_1 & ix_3 \end{pmatrix}$ and all operations in $\mathbb{R}^3$ can as well be carries out with the corresponding operations in $su(2)$. From now on the same notations will be used for vectors in $\mathbb{R}^3$ and their corresponding $su(2)$ matrices.

The scalar product induced from $\mathbb{R}^3$ can be calculated as

$$\langle x, y \rangle = -2tr(xy),$$

since then

$$\begin{aligned} \langle e_1, e_1 \rangle &= -2tr\left(\frac{1}{2}\begin{pmatrix} 0 & -i \\ -i & 0 \end{pmatrix} \cdot \frac{1}{2}\begin{pmatrix} 0 & -i \\ -i & 0 \end{pmatrix}\right) \\ &= -2tr\left(\frac{1}{4}\begin{pmatrix} -1 & 0 \\ 0 & -1 \end{pmatrix}\right) \\ &= 1 \end{aligned}$$

and similar

$$\langle e_2, e_2 \rangle = \langle e_3, e_3 \rangle = 1$$

as well as

$$\begin{aligned} \langle e_1, e_2 \rangle &= -2tr\left(\frac{1}{4}\begin{pmatrix} 0 & -i \\ -i & 0 \end{pmatrix} \cdot \begin{pmatrix} 0 & -1 \\ 1 & 0 \end{pmatrix}\right) \\ &= -2tr\left(\frac{1}{4}\begin{pmatrix} -i & 0 \\ 0 & i \end{pmatrix}\right) \\ &= 0 \end{aligned}$$

[3] This basis was chosen in such a way, that the matrix commutator will correspond to the cross product.

and similar

$$\langle e_2, e_3 \rangle = \langle e_1, e_3 \rangle = 0.$$

Defining the matrix commutator

$$[x, y] := xy - yx \quad x, y \in su(2),$$

then the corresponding vectors satisfy

$$x \times y = [x, y].$$

Proof.

$$\begin{aligned}
[x,y] &= xy - yx \\
&= \frac{1}{2}\begin{pmatrix} -ix_3 & -x_2 - ix_1 \\ x_2 - ix_1 & ix_3 \end{pmatrix} \frac{1}{2}\begin{pmatrix} -iy_3 & -y_2 - iy_1 \\ y_2 - iy_1 & iy_3 \end{pmatrix} \\
&\quad -\frac{1}{2}\begin{pmatrix} -iy_3 & -y_2 - iy_1 \\ y_2 - iy_1 & iy_3 \end{pmatrix} \frac{1}{2}\begin{pmatrix} -ix_3 & -x_2 - ix_1 \\ x_2 - ix_1 & ix_3 \end{pmatrix} \\
&= \frac{1}{4}\begin{pmatrix} -x_3y_3 - x_2y_2 - x_1y_1 - i(x_1y_2 - x_2y_1) & -(x_3y_1 - x_1y_3) - i(x_2y_3 - x_3y_2) \\ (x_3y_1 - x_1y_3) - i(x_2y_3 - x_3y_2) & -x_3y_3 - x_2y_2 - x_1y_1 + i(x_1y_2 - x_2y_1) \end{pmatrix} \\
&\quad -\frac{1}{4}\begin{pmatrix} -x_3y_3 - x_2y_2 - x_1y_1 + i(x_1y_2 - x_2y_1) & (x_3y_1 - x_1y_3) + i(x_2y_3 - x_3y_2) \\ -(x_3y_1 - x_1y_3) + i(x_2y_3 - x_3y_2) & -x_3y_3 - x_2y_2 - x_1y_1 - i(x_1y_2 - x_2y_1) \end{pmatrix} \\
&= \frac{1}{2}\begin{pmatrix} -i(x_1y_2 - x_2y_1) & -(x_3y_1 - x_1y_3) - i(x_2y_3 - x_3y_2) \\ (x_3y_1 - x_1y_3) - i(x_2y_3 - x_3y_2) & i(x_1y_2 - x_2y_1) \end{pmatrix} \\
&\overset{\substack{vector \\ form}}{=} \begin{pmatrix} x_2y_3 - x_3y_2 \\ x_3y_1 - x_1y_3 \\ x_1y_2 - x_2y_1 \end{pmatrix} \\
&= x \times y
\end{aligned}$$

□

Further note that

$$e_i e_j = \frac{1}{2}\varepsilon_{ijk} e_k \tag{3.1}$$

where ε_{ijk} is the totally antisymmetric tensor with $\varepsilon_{012} = 1$.

3.2.2 The matrix group $SU(2)$

The set of unitary two by two matricis with determinant one

$$SU(2) := \{A \in gl(2, \mathbb{C}), A^* A = Id,\ det(A) = 1\}$$

is a matrix group, with which rotations in $\mathbb{R}^3$ can be conveniently described:

Theorem 3.4. *A vector $X \in \mathbb{R}^3$ rotated around a unit vector*[4] $V \in \mathbb{R}^3, \langle V, V \rangle = 1$ *by the angle $\alpha \in \mathbb{R}$ can be described in terms of $su(2)$ and $SU(2)$ as*

$$X \mapsto \Phi^{-1} X \Phi \in su(2),$$

where $SU(2) \ni \Phi = \cos\frac{\alpha}{2} \cdot Id(2) + \sin\frac{\alpha}{2} V$. $\Phi, \widetilde{\Phi} \in SU(2)$ describe the same rotation if and only if they satisfy $\Phi = \pm\widetilde{\Phi}$.

[4] Or more precisely around the axis through the origin spanned by V.

Proof. Omitted here, see e. g. [B06]. $\square$

Theorem 3.5. *Let $F = (N, B, T) : [t_0, t_1] \to SO(3)$ be a differentiable motion*[5] *in $\mathbb{R}^3$, then*

1. *there exists a differentiable $\Phi : [t_0, t_1] \to SU(2)$ with*

$$\begin{array}{ccc} N & \leftrightarrow & \Phi^{-1}e_1\Phi \\ B & \leftrightarrow & \Phi^{-1}e_2\Phi \\ T & \leftrightarrow & \Phi^{-1}e_3\Phi. \end{array}$$

2. *$\Phi : [t_0, t_1] \to SU(2)$ is unique up to the transformation $\Phi \mapsto -\Phi$.*

3. *Φ satisfies $\Phi' = U\Phi$ where $U = \kappa_2 e_1 - \kappa_1 e_2 - \tau e_3 \in su(2)$ and*

$$\begin{array}{cccl} \kappa_1 & := & \langle T', N\rangle & \textit{is the geodesic curvature,} \\ \kappa_2 & := & \langle T', B\rangle & \textit{the normal curvature and} \\ \tau & := & \langle N', B\rangle & \textit{the torsion} \end{array}$$

of the frame.

Proof. Only *3.* will be proved here. Define therefore $U := \Phi'\Phi^{-1}$ and show first $U \in su(2)$. For every invertible operator holds

$$\begin{array}{rcl} \Phi\Phi^{-1} = Id & \overset{diff.}{\Rightarrow} & \Phi'\Phi^{-1} + \Phi(\Phi^{-1})' = 0 \\ & \Rightarrow & (\Phi^{-1})' = -\Phi^{-1}\Phi'\Phi^{-1}, \end{array}$$

together with

$$\Phi \in SU(2) \quad \Rightarrow \quad \Phi^* = \Phi^{-1}$$

yields

$$\begin{array}{rcl} (\Phi'\Phi^{-1})^* & = & (\Phi^{-1})^*(\Phi')^* \\ & = & \Phi(\Phi')-1 \\ & = & \Phi(\Phi-1)' \\ & = & -\Phi\Phi^{-1}\Phi'\Phi^{-1} \\ & = & -\Phi'\Phi^{-1}. \end{array}$$

Further using

$$t \mapsto A(t),\ A(t_0) = Id \Rightarrow \frac{\mathrm{d}}{\mathrm{d}t} det A(t)\bigg|_{t=t_0} = tr(A'(t_0))$$

one gets

$$\begin{array}{rcl} tr(\Phi'\Phi^{-1}) & = & \dfrac{\mathrm{d}}{\mathrm{d}t} det(\Phi(t)\Phi^{-1}(t_0))\bigg|_{t=t_0} \\ & = & \dfrac{\mathrm{d}}{\mathrm{d}t} \underbrace{det(\Phi(t))}_{=1}\underbrace{det(\Phi^{-1}(t_0))}_{=const.}\bigg|_{t=t_0} \\ & = & 0 \end{array}$$

[5] (N, B, T) is a positive oriented orthonormal basis $\forall t \in [t_0, t_1]$.

and $U \in su(2)$. Therefore $U = a \cdot e_1 + b \cdot e_2 + c \cdot e_3$ with

$$\begin{aligned} a &= \langle U, e_1 \rangle \\ b &= \langle U, e_2 \rangle \\ c &= \langle U, e_3 \rangle . \end{aligned}$$

But

$$\begin{aligned} \kappa_1 &= \langle T', N \rangle \\ &= \left\langle (\Phi^{-1} e_3 \Phi)', \Phi^{-1} e_1 \Phi \right\rangle \\ &= -2tr\Big((\Phi^{-1} e_2 \Phi' + (\Phi^{-1})' e_2 \Phi) \Phi^{-1} e_1 \Phi \Big) \\ &= -2tr(\Phi^{-1} e_3 \Phi' \Phi^{-1} e_1 \Phi - \Phi^{-1} \Phi' \Phi^{-1} e_3 e_1 \Phi) \\ &\overset{tr(B^{-1}AB)=tr(A)}{=} -2tr(e_3 U e_1 - U e_3 e_1) \\ &\overset{tr(AB)=tr(BA)}{=} -2tr(U e_1 e_3 - U e_3 e_1) \\ &\overset{3.1}{=} -2tr(-U\frac{e_2}{2} - U\frac{e_2}{2}) \\ &= 2tr(U e_2) \\ &= -\langle U, e_2 \rangle \\ &= -b \end{aligned}$$

and similar

$$\kappa_2 = a, \ \tau = -c$$

and therefore

$$U = \kappa_2 e_1 - \kappa_1 e_2 - \tau e_3 .$$

□

Lemma 3.6. *Let $(N, B, T) : [t_0, t_1] \mapsto SO(3)$ and $\Phi : [t_0, t_1] \mapsto SU(2)$ be corresponding rotations as above, Ω its vector of angular velocity in the body frame and ω in the rest frame, then*

$$\Omega = -\Phi' \Phi^{-1} \tag{3.2}$$

$$\omega = -\Phi^{-1} \Phi' \tag{3.3}$$

Proof. On the one hand by definition

$$N' = \omega \times N = [\omega, N],$$

on the other hand

$$\begin{aligned} N' &= (\Phi^{-1} e_1 \Phi)' \\ &= -\Phi^{-1} \Phi' \Phi^{-1} e_1 \Phi + \Phi^{-1} e_1 \Phi' \\ &= \Phi^{-1} e_1 \Phi \Phi^{-1} \Phi' - \Phi^{-1} \Phi' \Phi^{-1} e_1 \Phi \\ &= [\Phi^{-1} e_1 \Phi, \Phi^{-1} \Phi'] = [N, \Phi^{-1} \Phi'] \\ &= [-\Phi^{-1} \Phi', N], \end{aligned}$$

which shows 3.3. Since $\Omega = \Phi \omega \Phi^{-1}$, see theorem 3.4 part 1., we immediately get 3.2. □

3.3 Energy of the spinning top

By corollary 2.11 the kinetic energy of a rigid body fixed at 0 is

$$T = \frac{1}{2}\left\langle \omega, J_{restframe} \cdot \omega \right\rangle .$$

Since the scalar product does not change under a rotation the kinetic energy expressed in the body frame is

$$T = \frac{1}{2}\left\langle \Omega, J\Omega \right\rangle .$$

where Ω is the vector of angular velocity and J the inertia tensor in the body frame (N, B, T), i. e.

$$J = \begin{pmatrix} I_N & 0 & 0 \\ 0 & I_B & 0 \\ 0 & 0 & I_T \end{pmatrix}$$

with I_N, I_B, I_T the principal moments of inertia. Therefore

$$T = \frac{1}{2}(I_N\Omega_N^2 + I_B\Omega_B^2 + I_T\Omega_T^2).$$

The potential energy of the body is

$$U = \mathcal{M} \cdot g \cdot h$$

where $\mathcal{M}$ is the total mass of the body, g the gravity constant and h the height of the center of mass a of the body[6].

Given a gravity vector p pointing in the (positive) third coordinate direction of the rest frame and having length g

$$p = g \cdot e_3,$$

further given the center of mass

$$\begin{aligned} a &= A_N \cdot N + A_B \cdot B + A_T \cdot T \\ &= a_1 \cdot e_2 + a_2 \cdot e_3 + a_3 \cdot e_3, \end{aligned} \tag{3.4}$$

((e_1, e_2, e_3) being the rest frame), one gets

$$U = \mathcal{M} \cdot \langle p, a \rangle = \mathcal{M} \cdot g \cdot a_3.$$

Finally the Lagrange function is

$$L = T - U = \frac{1}{2}(I_N\Omega_N^2 + I_B\Omega_B^2 + I_T\Omega_T^2) - \mathcal{M} \cdot \langle p, a \rangle . \tag{3.5}$$

3.4 Equation of motion of the spinning top in the rest frame

Let the position of the quader be $\Phi : [t_0, t_1] \to SU(2), t \mapsto \Phi(t)$, then a variation of the position is

$$\Phi : [t_0, t_1] \times [-\epsilon, \epsilon] \longrightarrow SU(2)$$

$$(t, \varepsilon) \longmapsto \Phi_\varepsilon(t, \varepsilon) := \Phi(t)H(t, \varepsilon)$$

[6]The homogeneous gravity field acts on the body as if the body had all its mass concentrated at the center of mass.

where

$$H : [t_0, t_1] \times [-\epsilon, \epsilon] \longrightarrow SU(2)$$

is differentiable and satisfies

$$H(t_0, \varepsilon) = H(t_1, \varepsilon) = H(t, 0) = Id \quad \forall t, \varepsilon. \tag{3.6}$$

Under the variation only the body frame- and rest frame coordinates change. Giving proper notations and expressing the Lagrange function in body frame coordinates one gets

$$\begin{aligned} L_\varepsilon &= \frac{1}{2}(I_N \Omega^2_{N_\varepsilon,\varepsilon} + I_B \Omega^2_{B_\varepsilon,\varepsilon} + I_T \Omega^2_{T_\varepsilon,\varepsilon}) - \mathcal{M} \cdot \langle p, a_\varepsilon \rangle \\ &= \frac{1}{2}(I_N \langle \omega_\varepsilon, N_\varepsilon \rangle^2 + I_B \langle \omega_\varepsilon, B_\varepsilon \rangle^2 + I_T \langle \omega_\varepsilon, T_\varepsilon \rangle^2) \\ &\quad - \mathcal{M} \cdot \langle p, A_N \cdot N_\varepsilon + A_B \cdot B_\varepsilon + A_T \cdot T_\varepsilon \rangle \\ &= \left\langle \left(\frac{1}{2} I_N \langle \omega_\varepsilon, N_\varepsilon \rangle \omega_\varepsilon - \mathcal{M} \cdot A_N \cdot p \right), N_\varepsilon \right\rangle \\ &\quad + \left\langle \left(\frac{1}{2} I_B \langle \omega_\varepsilon, B_\varepsilon \rangle \omega_\varepsilon - \mathcal{M} \cdot A_B \cdot p \right), B_\varepsilon \right\rangle \\ &\quad + \left\langle \left(\frac{1}{2} I_T \langle \omega_\varepsilon, T_\varepsilon \rangle \omega_\varepsilon - \mathcal{M} \cdot A_T \cdot p \right), T_\varepsilon \right\rangle \end{aligned} \tag{3.7}$$

By theorem 3.1 and lemma 3.2 the motion of the spinning top satisfies

$$0 = \frac{\mathrm{d}}{\mathrm{d}\varepsilon} \int_{t_0}^{t_1} L_\varepsilon \, \mathrm{d}t \Big|_{\varepsilon=0} \tag{3.8}$$

which is to be calculated in this chapter.

But first some observations. Denote

$$\eta := \frac{\partial H(t,\varepsilon)}{\partial \varepsilon}\Big|_{\varepsilon=0},$$

then from theorem 3.5 and equation (3.6) follows $\eta \in su(2)$.

Further it follows from (3.6) that

$$\eta(t_0) = \eta(t_1) = 0,$$

$$H'\Big|_{\varepsilon=0} = 0$$

and

$$\frac{\partial H^{-1}}{\partial \varepsilon}\Big|_{\varepsilon=0} = -\eta.$$

With that one gets for the variation of the vector of angular velocity

$$
\begin{aligned}
\omega_\varepsilon &\overset{3.3}{=} -\Phi_\varepsilon^{-1}\Phi_\varepsilon' \\
&= -(\Phi H)^{-1}(\Phi H)' \\
&= -H^{-1}\Phi^{-1}(\Phi' H + \Phi H') \\
&= H^{-1}(-\Phi^{-1}\Phi')H - H^{-1}H' \\
&= H^{-1}\omega H - H^{-1}H' \\
\Rightarrow \frac{\partial \omega_\varepsilon}{\partial \varepsilon} &= \left(H^{-1}\omega \frac{\partial H}{\partial \varepsilon} + \frac{\partial H^{-1}}{\partial \varepsilon}\omega H - \frac{\partial H^{-1}}{\partial \varepsilon} H' - H^{-1}\frac{\partial H'}{\partial \varepsilon} \right)\bigg|_{\varepsilon=0} \\
&= \omega\eta - \eta\omega - \eta' \\
&= [\omega, \eta] - \eta'.
\end{aligned}
$$

Furthermore

$$
\begin{aligned}
N_\varepsilon &= \Phi_\varepsilon^{-1} e_1 \Phi_\varepsilon \\
&= H^{-1}\Phi^{-1} e_2 \Phi H \\
&= H^{-1} N H \\
\Rightarrow \frac{\partial N_\varepsilon}{\partial \varepsilon}\bigg|_{\varepsilon=0} &= \left(H^{-1} N \frac{\partial H}{\partial \varepsilon} + \frac{\partial H^{-1}}{\partial \varepsilon} N H \right)\bigg|_{\varepsilon=0} \\
&= [N, \eta]
\end{aligned}
$$

and analog

$$
\frac{\partial B_\varepsilon}{\partial \varepsilon}\bigg|_{\varepsilon=0} = [B, \eta], \quad \frac{\partial T_\varepsilon}{\partial \varepsilon}\bigg|_{\varepsilon=0} = [T, \eta].
$$

Now equation (3.8) can be solved. The calculation is carried out for the N-component of the Lagrange function, the others are analog.

$$
\begin{aligned}
0 \quad &= \quad \frac{\mathrm{d}}{\mathrm{d}\varepsilon} \int_{t_0}^{t_1} \left\langle \Big(\frac{1}{2} I_N \left\langle \omega_\varepsilon, N_\varepsilon \right\rangle \omega_\varepsilon - \mathcal{M} \cdot A_N \cdot p \Big), N_\varepsilon \right\rangle \,\mathrm{d}t \Big|_{\varepsilon=0} \\
&= \quad \int_{t_0}^{t_1} \left\langle \frac{\mathrm{d}}{\mathrm{d}\varepsilon} \Big(\frac{1}{2} I_N \left\langle \omega_\varepsilon, N_\varepsilon \right\rangle \omega_\varepsilon - \mathcal{M} \cdot A_N \cdot p \Big), N_\varepsilon \right\rangle + \\
& \quad\quad \left\langle \Big(\frac{1}{2} I_N \left\langle \omega_\varepsilon, N_\varepsilon \right\rangle \omega_\varepsilon - \mathcal{M} \cdot A_N \cdot p \Big), \frac{\mathrm{d}}{\mathrm{d}\varepsilon} N_\varepsilon \right\rangle \,\mathrm{d}t \Big|_{\varepsilon=0} \\
&= \quad \int_{t_0}^{t_1} \left\langle \frac{1}{2} I_N \Big(\left\langle \omega_\varepsilon, N_\varepsilon \right\rangle \frac{\mathrm{d}}{\mathrm{d}\varepsilon} \omega_\varepsilon + \left\langle \frac{\mathrm{d}}{\mathrm{d}\varepsilon} \omega_\varepsilon, N_\varepsilon \right\rangle \omega_\varepsilon + \left\langle \omega_\varepsilon, \frac{\mathrm{d}}{\mathrm{d}\varepsilon} N_\varepsilon \right\rangle \omega_\varepsilon \Big), N_\varepsilon \right\rangle \Big|_{\varepsilon=0} + \\
& \quad\quad \left\langle \Big(\frac{1}{2} I_N \left\langle \omega, N \right\rangle \omega - \mathcal{M} \cdot A_N \cdot p \Big), [N, \eta] \right\rangle \,\mathrm{d}t \\
&= \quad \int_{t_0}^{t_1} \left\langle \frac{1}{2} I_N \Big(\left\langle \omega, N \right\rangle ([\omega, \eta] - \eta') + \left\langle [\omega, \eta] - \eta', N \right\rangle \omega + \left\langle \omega, [N, \eta] \right\rangle \omega, N \right\rangle + \\
& \quad\quad \frac{1}{2} I_N \left\langle \omega, N \right\rangle \left\langle [\eta, \omega], N \right\rangle - \left\langle \mathcal{M} \cdot A_N \cdot [p, N], \eta \right\rangle \,\mathrm{d}t \\
&= \quad \int_{t_0}^{t_1} \frac{1}{2} I_N \left\langle \omega, N \right\rangle \Big(\left\langle [\omega, \eta], N \right\rangle - \left\langle \eta', N \right\rangle + \left\langle [\omega, \eta], N \right\rangle - \left\langle \eta', N \right\rangle + \left\langle [\eta, \omega], N \right\rangle + \\
& \quad\quad \left\langle [\eta, \omega], N \right\rangle \Big) - \left\langle \mathcal{M} \cdot A_N \cdot [p, N], \eta \right\rangle \,\mathrm{d}t \\
&= \quad \int_{t_0}^{t_1} \left\langle I_N \left\langle \omega, N \right\rangle N, -\eta' \right\rangle \,\mathrm{d}t - \int_{t_0}^{t_1} \left\langle \mathcal{M} \cdot A_N \cdot [p, N], \eta \right\rangle \,\mathrm{d}t \\
&\overset{part.\ Int.}{=} \quad \left\langle I_N \left\langle \omega, N \right\rangle N, -\eta \right\rangle \Big|_{t_0}^{t_1} + \int_{t_0}^{t_1} \left\langle I_N \Big(\left\langle \omega, N \right\rangle N' + \left\langle \omega', N \right\rangle N + \langle \omega, \underbrace{N'}_{=\omega \times N} \rangle N \Big), \eta \right\rangle \,\mathrm{d}t \\
& \quad\quad - \int_{t_0}^{t_1} \left\langle \mathcal{M} \cdot A_N \cdot [p, N], \eta \right\rangle \,\mathrm{d}t \\
&\overset{\eta(t_0)=\eta(t_1)=0}{=} \quad \int_{t_0}^{t_1} \left\langle I_N (\left\langle \omega, N \right\rangle N' + N N^t \cdot \omega') - \mathcal{M} \cdot A_N \cdot [p, N], \eta \right\rangle \,\mathrm{d}t
\end{aligned}
$$

In the vector form this is

$$
0 = \int_{t_0}^{t_1} \left\langle I_N (\left\langle \omega, N \right\rangle N' + N N^t \cdot \omega') - \mathcal{M} \cdot A_N \cdot p \times N, \eta \right\rangle \,\mathrm{d}t.
$$

Since the direction of variation η is arbitrary one can use lemma 3.3 and gets

$$
0 = I_N (\left\langle \omega, N \right\rangle N' + N N^t \cdot \omega') - \mathcal{M} \cdot A_N \cdot p \times N.
$$

Including all three coordinates this gets

$$\begin{aligned}
0 &= I_N(\langle\omega, N\rangle N' + NN^t \cdot \omega') + I_B(\langle\omega, B\rangle B' + BB^t \cdot \omega') + I_T(\langle\omega, T\rangle T' + TT^t \cdot \omega') \\
&\quad -\mathcal{M} \cdot p \times (A_N \cdot N + A_B \cdot B + A_T \cdot T) \\
&= (\overbrace{I_N \cdot NN^t + I_B \cdot BB^t + I_T \cdot TT^t}^{=:A})\omega' + I_N \langle\omega, N\rangle \omega \times N \\
&\quad +I_B \langle\omega, B\rangle \omega \times B + I_T \langle\omega, T\rangle \omega \times T - \mathcal{M} \cdot p \times a \\
\Leftrightarrow A\omega' &= (I_N \cdot NN^t + I_B \cdot BB^t + I_T \cdot TT^t)\omega \times \omega + \mathcal{M} \cdot p \times a \\
\Leftrightarrow \omega' &\overset{(*)}{=} A^{-1}(A\omega \times \omega + \mathcal{M} \cdot p \times a) \qquad (3.9)
\end{aligned}$$

This is the desired equation of motion of the spinning top and together with (by definition)

$$N' = \omega \times N, \quad B' = \omega \times B, \quad B' = \omega \times B$$

solved numerically and visualized in the *Top Visualization* program.

In $(*)$ was used that:

Lemma 3.7. *A is invertible.*

Proof. Let $v \in \mathbb{R}^3 \backslash \{0\}$ arbitrary. Then, with $I_N, I_B, I_T > 0$,

$$\begin{aligned}
v^T Av &= I_N v^T NN^T v + I_B v^T BB^T v + I_T v^T TT^T v \\
&= I_N (\sum_{i=1}^{3} N_i v_i)^2 + I_B (\sum_{i=1}^{3} B_i v_i)^2 + I_T (\sum_{i=1}^{3} T_i v_i)^2 \\
&= I_N \langle v, N\rangle^2 + I_B \langle v, B\rangle^2 + I_T \langle v, T\rangle^2 \\
&= I_N v_N^2 + I_B v_B^2 + I_T v_T^2 \\
&> 0.
\end{aligned}$$

Hence A is positive definite and invertible. □

Remark. Another form of equations of motion of a rigid body around a fixed point are Kirchhoffs equations

$$\begin{aligned}
\dot{M} &= M \times (J^{-1}M) + \mathcal{M} \cdot P \times A \\
\dot{P} &= P \times (J^{-1}M),
\end{aligned}$$

where all vectors are expressed in the body frame.

For computing numerical solutions, using them has a serious disadvantage. When e. g. approximating a solution at time $t + \varepsilon$ based on given initial data at time t, numerical algorithms evaluate the differential equations at multiple points within the interval $[t, t + \varepsilon]$. In body frame formulation, the frame stays constant and can be integrated to the new body frame at time $t+\varepsilon$ just using $\omega(t)$. The present knowledge about M and hence ω at the additional points within the interval $[t, t + \varepsilon]$ is lost.

This can be improved by a formulation of the equations of motion in rest frame coordinates, so they can be solved simultaneously with the motion of the body frame expressed in the rest frame. I. e. solving the first order system of ordinary differential equations

$$\begin{aligned}
\omega' &= A^{-1}(A\omega \times \omega + \mathcal{M} \cdot p \times a) \\
N' &= \omega \times N \\
B' &= \omega \times B \\
T' &= \omega \times T
\end{aligned}$$

simultaneously yields far better results, even though the integrability of the last three equations is not used by numerical methods.

3.5 Elastic curves and spinning tops

Definition. A *framed curve* is an immersed[7], arclength parametrized[8] curve $\gamma : [0, L] \to \mathbb{R}^3$ with a unit normalfield $N : [0, L] \to S^2$. $(N, B := T \times N, T := \gamma')$ is the (orthonormal) frame of the curve.

Denote the values

$$\begin{array}{rcll} \kappa_1 & := & \langle T', N \rangle & \text{geodesic curvature} \\ \kappa_2 & := & \langle T', B \rangle & \text{normal curvature} \\ \tau & := & \langle N', B \rangle & \text{torsion.} \end{array}$$

Definition. A framed curve γ delivering an extremal

- to the functional
$$S = \int_0^L \kappa_1^2 + \kappa_2^2 + \alpha\tau^2 \,\mathrm{d}x,$$
is called an *isotropic elastic curve* or *isotropic elastic rod*,

- to the functional
$$S = \int_0^L \alpha_1\kappa_1^2 + \alpha_2\kappa_2^2 + \alpha\tau^2 \,\mathrm{d}x,$$
is called an *anisotropic elastic curve* or *anisotropic elastic rod*,

where $\alpha, \alpha_1, \alpha_2 \in \mathbb{R}$, the boundary points $\gamma(0)$ and $\gamma(L)$ and the frames (N, B, T) at the boundary points are fixed.

Remark. Physically those are rods that exert a resistance against bending and twisting. α is in both cases the resistance against twisting. The isotropic elastic curve exerts the same resistance against bending the rod in N or B direction, meaning that the cross section of the rod is symmetric. In the anisotropic case α_1 and α_2 give different resistances like e. g. at a rod with rectangular cross section. See figures 3.1(a) and 3.1(b).

The boundary conditions make finding elastic curves an extremal problem with constraints. The condition of fixed boundary points can be formulated as

$$\int_0^L T \,\mathrm{d}x - \Big(\gamma(L) - \gamma(0)\Big) = 0$$

and included in the functional with the Lagrange multiplier $2b \in \mathbb{R}^3$ as[9]

$$S = \int_0^L \kappa_1^2 + \kappa_2^2 + \alpha\tau^2 + \langle 2b, T \rangle \,\mathrm{d}x$$

[7] Equivalence class of regular (non-zero derivative) parametrisations of the curve.
[8] $\|\gamma'\| \equiv 1$.
[9] The constant part of the condition has no influence on the variational problem.

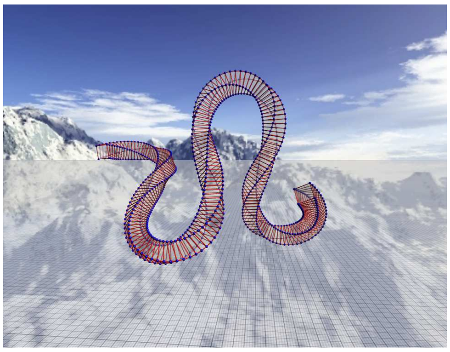

(a) Isotropic elastic curve.

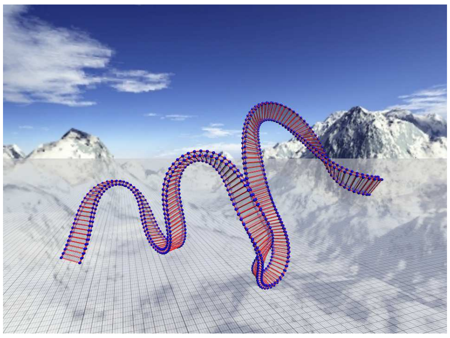

(b) Anisotropic elastic curve.

Figure 3.1: Elastic curves.

respectively

$$S = \int_0^L \alpha_1\kappa_1^2 + \alpha_2\kappa_2^2 + \alpha\tau^2 + \langle 2b, T\rangle \,\mathrm{d}x.$$

To establish a connection between elastic curves and spinning tops the problem is reformulated in terms of $su(2)$ and $SU(2)$ again.

As stated in theorem 3.5 for every framed curve γ there exists a unique rotation

$$\Phi : [0, L] \to SU(2)$$

taking the rest frame (e_1, e_2, e_3) to (N, B, T)[10]:

$$N = \Phi^{-1}e_1\Phi, \quad B = \Phi^{-1}e_2\Phi, \quad T = \Phi^{-1}e_3\Phi$$

Then

$$\begin{aligned} N' &= (\Phi^{-1})'e_1\Phi + \Phi^{-1}e_1\Phi' \\ &= \Phi^{-1}e_1\Phi'\Phi^{-1}\Phi - \Phi^{-1}\Phi'\Phi^{-1}e_1\Phi \\ &= \Phi^{-1}[e_1, \Phi'\Phi^{-1}]\Phi \end{aligned}$$

and similarly

$$B' = \Phi^{-1}[e_2, \Phi'\Phi^{-1}]\Phi, \quad T' = \Phi^{-1}[e_3, \Phi'\Phi^{-1}]\Phi.$$

By lemma 3.6 $\Omega = -\Phi'\Phi^{-1}$ is the vector of angular velocity in the body frame, $\Omega = (\Omega_N, \Omega_B, \Omega_T)$, and one gets

$$\kappa_1 = \langle T', N\rangle = \left\langle \Phi^{-1}[e_3, \Phi'\Phi^{-1}]\Phi, \Phi^{-1}e_1\Phi \right\rangle = \left\langle [-\Phi'\Phi^{-1}, e_3], e_1 \right\rangle = \langle \Omega \times e_3, e_1\rangle = \Omega_B$$

and similarly

$$\kappa_2 = -\Omega_N, \quad \tau = \Omega_T,$$

so that the functional gets

$$S = \int_0^L \Omega_N^2 + \Omega_B^2 + \alpha\Omega_T^2 + \langle 2b, T\rangle \,\mathrm{d}x \tag{3.10}$$

[10] All expressed in $su(2)$.

respectively

$$S = \int_0^L \alpha_1 \Omega_N^2 + \alpha_2 \Omega_B^2 + \alpha \Omega_T^2 + \langle 2b, T \rangle \, \mathrm{d}x. \tag{3.11}$$

So elastic curves deliver an extremals to those functionals while the frames at the boundary points $\Phi(0)$ and $\Phi(L)$ are fixed during variation.

But (3.11) is exactly twice the Lagrange function of the spinning top (3.5) if and only if the center of mass of the top a is parallel to T; then $b = \|a\| \cdot p$ and $\alpha_1, \alpha_2, \alpha$ take the roll of the principal moments of inertia. And since the constant factor 2 does not change the extremals of the functional, it holds:

Theorem 3.8. *The paths of body frames of spinning tops with the center of mass on one of its principal axes is in a one-to-one correspondence to frames of anisotropic elastic curves.*

Since for the Lagrange top $I_N = I_B$ and $a \| T$, (3.10) multiplied by $2I_n$ gets (3.5) and one has the special case of:

Theorem 3.9 (Kirchhoffs kinetic analogy)**.** *The paths of Lagrange top body frames are in a one-to-one correspondence to frames of isotropic elastic curves.*

These analogies are visualized in the *Top Visualization* program as described in section 5.7.

Chapter 4

Discretizations

4.1 Numerical discretizations

The path of the spinning top is an ordinary differential equation (ODE), it depends only on time. In numerical analysis there are various methods of approximating the solutions of ODEs by approximating its derivatives with the help of finite differences. Depending on the chosen method and the given tolerance parameters, these solutions are more or less accurate. But in general they do not use the fact, that in Hamiltonian systems there is an underlying structure that could give more information about the motion. This is one disadvantage of numerical discretizations compared to the integrable discretization described in the next section.

Further, for a given time discretization step length parameter ε, numerical discretizations evaluate the ODE several times at points in the interval $[t, t+\varepsilon]$, making them much more demanding in terms of calculation time and memory.

4.1.1 Extrap - The Gragg-Burlisch-Stoer extrapolation algorithm

In the *Top Visualization* program described in chapter 5 the integrable discretization is compared to the *Gragg-Burlisch-Stoer extrapolation algorithm* that will be called *Extrap* in this thesis and in the program.

The algorithm is based on the explicit midpoint rule with step size control and order selection, see [HNW]. It is a very modern, probably one of the most sophisticated methods for solving ODEs.

Error tolerances and step size control Some details of the *Extrap* method from [HNW] are cited here in order to clarify the used error tolerances and the funcionality of the step size control.

Let therefore

$$
\begin{aligned}
\dot{y}_1(t) &= f_1(y_1(t), \ldots, y_n(t), t) \\
&\vdots \\
\dot{y}_n(t) &= f_n(y_1(t), \ldots, y_n(t), t)
\end{aligned}
$$

be a system of n ordinary first order differential equations,

$$h \in \mathbb{R}_+$$

be an initial step size length (which may be chosen by the user) and

$$t_0,\ y_i(t_0) \in \mathbb{R}$$

be the given initial data. Then the *Extrap* method calculates two approximations $\widetilde{y}(t_0+h)$ and $\widehat{y}(t_0+h)$ of $y(t_0+h)$ based on estimation of the derivatives of the y_i with the help of finite differences. Then an estimate of the error for the less precise result is $\widetilde{y}(t_0+h) - \widehat{y}(t_0+h)$. Now the user wants that error to satisfy

$$|\widetilde{y}(t_0+h) - \widehat{y}(t_0+h)| \leq sc_i, \quad sc_i := Atol_i + \max(|\widetilde{y}(t_0+h)|, |\widehat{y}(t_0+h)|) \cdot Rtol_i.$$

Relative errors are considered for $Atol_i = 0$, absolute errors for $Rtol_i = 0$. Usually both are different from zero in order to have a reasonable error tolerance independant of the values of y_i. As a measure of the error the *Extrap* method takes

$$err = \sqrt{\frac{1}{n}\sum_{i=1}^{n}\left(\frac{\widetilde{y}(t_0+h) - \widehat{y}(t_0+h)}{sc_i}\right)^2}.$$

Then if $err < 1$ the step is accepted and a new step size is determined, depending on how small err was. For details see [HNW]. If $err \geq 1$ the step is rejected and a smaller step size determined, with which the result will probably fulfill the required error tolerances.

When the *Extrap* method is applied to a quader in chapters 5 and 6 the tolerances are taken equal for all components, i. e. $Atol_i = Atol,\ Rtol_i = Rtol,\ \forall i = 1,\ldots,n$, and also $Atol = Rtol$ are taken equal.

4.2 Integrable discretization by A. I. Bobenko and Yu. B. Suris

This section gives an outline of the integrable time discretization of the Lagrange top as derived in [BS00], which will be called the *Bobenko-Suris discretization* in the present work. The derivations are made in a scaled coordinate system that simplifies certain quantities, this scaling is first demonstrated at the example of a quader. Then the used notations are recalled and finally the results that were implemented in the *Top Visualization* program are cited.

4.2.1 Calculation in a scaled coordinate system

Recalling that in the body frame a Lagrange top with coordinates as desribed in 2.5 has the inertia tensor[1]

$$J = \frac{\mathcal{M}}{3}\begin{pmatrix} {C_N}^2 + (2C_T)^2 & 0 & 0 \\ 0 & {C_N}^2 + (2C_T)^2 & 0 \\ 0 & 0 & 2{C_N}^2 \end{pmatrix},$$

with

$$\mathcal{M} = 8C_N C_B C_T = 8C_N^2 C_T$$

and center of mass coordinates

$$A = \begin{pmatrix} 0 \\ 0 \\ C_T \end{pmatrix},$$

one can simplify those by choosing appropriate units.

[1] In the Lagrange case $C_N = C_B$.

First scaling the length unit (calling the given length unit lu and the scaled one $\widetilde{lu}$) by

$$1\,\widetilde{lu} = C_T\,lu$$

the center of mass has coordinates

$$A = \begin{pmatrix} 0 \\ 0 \\ 1 \end{pmatrix},$$

wrt the scaled bodyframe $(\widetilde{e_1}, \widetilde{e_2}, \widetilde{e_3}) = C_T(e_1, e_2, e_3)$.

The (principal) moments of inertia have the unit $[lu^2\,mu]$, mu being the mass unit. Thus by scaling

$$1\,\widetilde{mu} = \frac{8C_N^2}{3C_T}(C_N^2 + C_T^2)\,mu$$

one gets in scaled coordinates

$$\begin{aligned} I_1 = I_2 &= \frac{\mathcal{M}}{3}(C_N^2 + C_T^2)\,lu^2\,mu \\ &= \frac{8C_N^2 C_T}{3}(C_N^2 + C_T^2)(\frac{1}{C_T}\,\widetilde{lu})^2(\frac{3C_T}{8C_N^2(C_N^2 + C_T^2)}\,\widetilde{mu}) \\ &= 1\,\widetilde{lu}^2\,\widetilde{mu} \end{aligned}$$

and

$$\begin{aligned} I_3 &= \frac{\mathcal{M}}{3}(2C_N^2)\,lu^2\,mu \\ &= \frac{2C_N^2}{C_N^2 + C_T^2}\,\widetilde{lu}^2\,\widetilde{mu}, \end{aligned}$$

so that in scaled coordinates

$$J = \begin{pmatrix} 1 & 0 & 0 \\ 0 & 1 & 0 \\ 0 & 0 & \frac{2C_N^2}{C_N^2 + C_T^2} \end{pmatrix}$$

or shorter

$$J = \begin{pmatrix} 1 & 0 & 0 \\ 0 & 1 & 0 \\ 0 & 0 & \alpha \end{pmatrix} \tag{4.1}$$

as used in [BS00].

Of course in this new units the vector of angular momentum m (respectively M) and the gravity vector p have new coordinates, namely

$$m = \begin{pmatrix} m_0 \\ m_1 \\ m_2 \end{pmatrix} \frac{mu\,lu^2}{s^2} = \frac{3}{8C_N^2 C_T(C_N^2 + C_T^2)} \begin{pmatrix} m_0 \\ m_1 \\ m_2 \end{pmatrix} \frac{\widetilde{mu}\,\widetilde{lu}^2}{s^2}$$

and M gets the same factor,

$$p = \begin{pmatrix} 0 \\ 0 \\ g \end{pmatrix} \frac{lu}{s^2} = \frac{1}{C_T} \begin{pmatrix} 0 \\ 0 \\ g \end{pmatrix} \frac{\widetilde{lu}}{s^2}.$$

The vector of angular velocity ω has the unit $\frac{1}{s^2}$ and therefore remains the same.

4.2.2 Notations

The calculations in [BS00] are carried out in the Lie group $SU(2)$ and the Lie algebra $su(2)$, as described in section 3.2.

Recalled in short, all used vectors in $\mathbb{R}^3$ are carried over to elements of $su(2)$ by the identification

$$\mathbb{R}^3 \ni x = \begin{pmatrix} x_1 \\ x_2 \\ x_3 \end{pmatrix} \leftrightarrow \frac{1}{2}\begin{pmatrix} -ix_3 & -x_2 - ix_1 \\ x_2 - ix_1 & ix_3 \end{pmatrix} \in su(2).$$

Rotations in $\mathbb{R}^3$ are identified with elements off $SU(2)$ according to theorem 3.4.

Now the notations used in [BS00] in the body frame[2] are

k	discrete time index, $k \in \mathbb{Z}$
ε	discrete time step length
a_k	center of mass at time k, in scaled units $\|a_k\| = 1 \quad \forall k$
p	gravity vector, $p = g \cdot e_2 = const.$
m_k	vector of angular momentum at time k
g_k	(rotation from rest- to) body frame at time k
$\mathbf{1}$	2×2 unit matrix
α	anisotropy parameter of the Lagrange top, see (4.1)
c	$c = \langle m_k, p\rangle$ integral of motion (like in every homogeneous gravity field)

4.2.3 Results

Now the *Bobenko-Suris discretization* is given by the following two theorems.

Theorem 4.1. *The discrete time evolution of a Lagrange top satisfies*

$$\begin{aligned} m_{k+1} &= m_k + \varepsilon[p, a_k] \\ a_{k+1} &= (\mathbf{1} + \varepsilon m_{k+1}) a_k (\mathbf{1} + \varepsilon m_{k+1})^{-1}. \end{aligned}$$

Theorem 4.2. *The discrete time evolution of the frame g_k can be determined from the linear difference equation*

$$g_{k+1} = w_k g_k,$$

where the w_k are given by

$$w_k = \frac{tr(w_k)}{2}(\mathbf{1} + \varepsilon \xi_k),$$

where

$$\begin{aligned} \xi_k &= m_{k+1} + c\frac{1-\alpha}{\alpha}\frac{a_{k+1} + a_k}{1 + \langle a_k, a_{k+1}\rangle} \\ &= \frac{2}{c}\frac{[a_k, a_{k+1}]}{1 + \langle a_k, a_{k+1}\rangle} + \frac{c}{\alpha}\frac{a_{k+1} + a_k}{1 + \langle a_k, a_{k+1}\rangle}, \end{aligned}$$

and

$$tr(w_k) = \frac{2}{\sqrt{1 + \frac{\varepsilon^2}{4}\langle \xi_k, \xi_k\rangle}} = \sqrt{2\frac{1 + \langle a_k, a_{k+1}\rangle}{1 + \varepsilon^2 c^2/4\alpha^2}}.$$

[2] Only the results in term of the body frame are used here.

This discretization is calculated and visualized in the *Top Visualization* program described in chapter 5.

Chapter 5

Calculation and the Top Visualization

This section is devoted to the actual calculation of the top motion and its visualization in the *Top Visualization* program. It can be found on the CD attached to the back cover or under http://www.math.tu-berlin.de/~bodack. It is also available as webstart application under http://www.math.tu-berlin.de/geometrie/ps/software.shtml. [1]

5.1 JReality

The *Top Visualization* program uses the jReality software [TBa], a 3D viewer in which the observer controls an avatar moving in a virtual environment and interacts with its content.

5.2 Move, look around, open panels

Move	W, A, S, D.
Look around	Hold the right mouse button and move the mouse.
Jump	SPACE.
Toggle gravity[2]	G.
VR settings panel	Doubleclick with the left mouse button on the scene floor. See section 5.3.
Top Visualization panel	Doubleclick with the left mouse button on the spinning top. See section 5.6.

5.3 Change jReality configuration

JReality configuration can be changed in the *VR settings* panel, see figure 5.1. It is opened with a doubleclick on the scene floor.

A detailed description of JReality can be found at www.jreality.de, in particular in the contained *Wiki*.

[1]Note that Java^{TM} Vs. 1.5 or higher is required. Also the program is rather intense in graphics and calculation, making it hard to use on slow systems.

[2]Not related to the gravity accelerating the top.

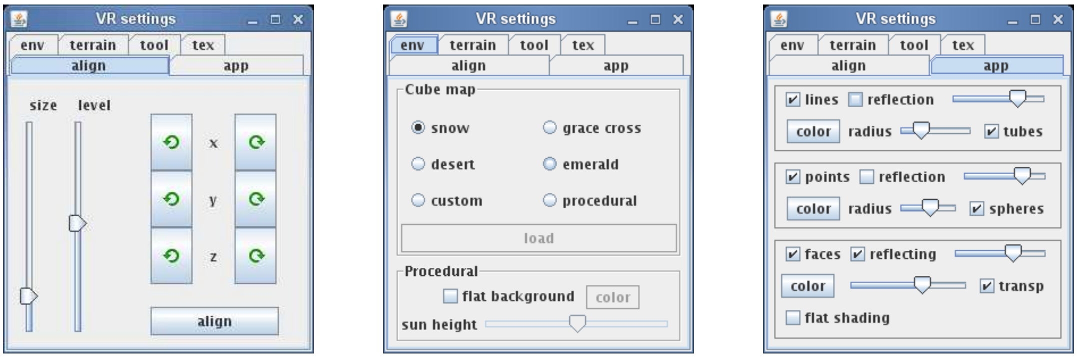

(a) Object position. (b) Scene background. (c) Object appearance.

Figure 5.1: JReality configurations.

5.3.1 2D view of the scene

One special option to change the view of the scene is included in the *Top Visualization panel*, see figure 5.2. The checkbox *view scene in (nearly) 2D* sets the position of the observer away from the object and increases the zoom factor. This way the contortion occurring in a 3D viewer is diminished.

5.4 Loaded content: A Lagrange top example

At startup the program loads a Lagrange top example like described in chapter 2, namely a quader with fixed point at the center of one of its faces and quader coordinates (C_N, C_N, C_T). See e. g. figure 2.5 for an explanation of these coordinates. The *Top Visualization panel* should be loaded and visible, too.

5.5 A first test run, the buttons *Start/Stop* and *Step*

Klick the *Step* or the *Start/Stop* button. The *Step* button makes the program calculate a single motion step, whereas the *Start/Stop* button starts a timer letting the program calculate the next step after every certain time period. This period is an internally stored variable called $delay$ which is indirectly editable with the *speed* slider described later in this chapter. Details of the used timer are given in section 5.8.5.

5.6 Change top and motion settings

The parameters of the top and its motion can be changed in the *Top Visualization panel*, see figure 5.2. Also various statistics are shown, depending on the loaded content.

5.6.1 Rotate quader

Left click, hold and drag the quader faces or edges.

The resulting rotation changes in the initial body frame, but keeps the quader coordinates.

5.6.2 Change size

Left click, hold and drag one of the points that are not at a corner of the face with the fixed point.

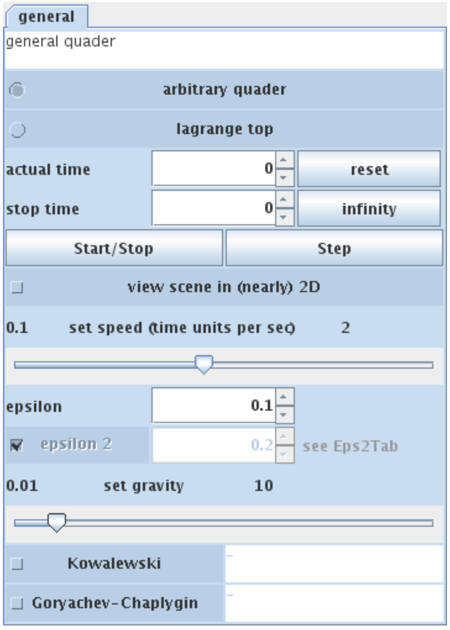

Figure 5.2: The *Top Visualization panel*. Here the parameters of the top and its motions can be set and various statistics are shown.

This changes the quader coordinates (C_N, C_B, C_T) in the body frame, see figure 2.5, and hence the mass

$$\mathcal{M} = 8 \cdot C_N \cdot C_B \cdot C_T$$

and also the moments of inertia, since the inertia tensor in the body frame is (see corollary 2.6)

$$J = \frac{\mathcal{M}}{3} \begin{pmatrix} {C_B}^2 + (2C_T)^2 & 0 & 0 \\ 0 & {C_N}^2 + (2C_T)^2 & 0 \\ 0 & 0 & {C_N}^2 + {C_B}^2 \end{pmatrix}.$$

5.6.3 Change fixed point

Click, hold and drag one of the quaders points with the middle mouse button. The origin stays the motions fixed point, the quaders position changes and effectively, seen from the quaders point of view, this corresponds to a quader motion wrt a changed fixed point.

While dragging the quader, the principal axes of inertia (the body frame) and the center of mass of the body are shown. See figure 5.3.

The principal axes and moments of inertia are calculated with the help of equation (2.14). Eigenvectors and Eigenvalues are calculated with the package [MTJ].

Remark. Changing the quaders fixed point is equivalent to changing its center of mass. This way, together with changing the quader coordinates, the geometry of every rigid body can be set, since it is determined by the body's center of mass and moments of inertia.

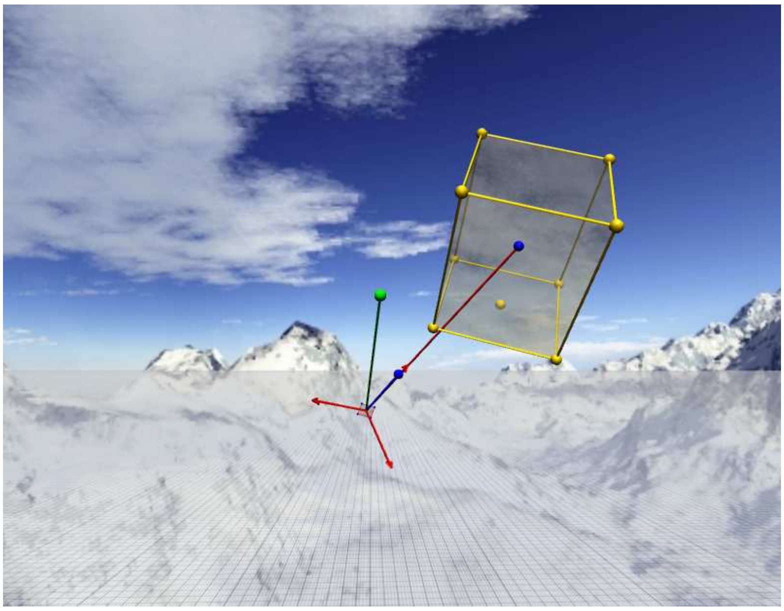

Figure 5.3: Example for a quader with an arbitrary fixed point. Moving the quader in the scene corresponds to changing its fixed point, seen from the quaders point of view.

5.6.4 Edit vector of kinetic momentum

Left click, hold and drag the tip[2] of the green vector.

The vector of angular velocity (blue) is automatically updated via formula (2.5).

5.6.5 Epsilon, speed and gravity

$Epsilon$ takes the role of the time discretization step length. E. g. the motion of a system traversing $t \in [0, 1]$ with an $epsilon = 0.02$ is approximated at $N = 50$ equidistant time points.

The $speed$ determines how fast the quader in the program should move. Effectively it sets a parameter

$$delay = \frac{1000\varepsilon}{speed} ms$$

of the timer described in section 5.8.5 and lets the program calculate a motion step more or less often.

The implementation of the timer allows only $delay \in \mathbb{N}$, which is assured by only accepting certain values for $speed$. The details are omitted here.

The *gravity* slider sets the length of the gravity vector, which points up in the scene, or in e_3-direction of the rest frame. (It is not visible in the *Top Visualization* program.) The higher the gravity the more the body is accelerated in negative e_3-direction.

[2]The point that is not the fixed point.

5.6.6 The Kowalewski and Goryachev-Chaplygin cases

Activating the corresponding checkbox edits the current quader such that it becomes a Kowalewski respectively Goryachev-Chaplygin case of rigid body motion. These are further [3] integrable spinning top cases:

Definition. The *Kowalewski* case is characterized by the principal moments of inertia satisfing $I_1 = I_2 = 2I_3$ and the center of mass lying in the plane spanned by the principal axes corresponding to I_1 and I_2.

In the *Goryachev-Chaplygin* case the center of mass lies in the same plane, the principal moments of inertia satisfy $I_1 = I_2 = 4I_3$ and additionally the vector of kinetic momentum is perpendicular to the gravity vector (or alternatively the third component of the vector of kinetic momentum in the rest frame m_3 is zero).

Denoting again the vector of angular momentum as $M = (M_1, M_2, M_3)$ and the gravity vector as $p = (p_1, p_2, p_3)$, then with appropriately scaled units the Hamiltonian[4] is in the *Kowalewski* case

$$H = \frac{1}{2}(M_1^2 + M_2^2 + 2M_3^2) - p_1$$

and has the additional integral

$$K = (M_1^2 - M_2^2 + 2p_1)^2 + 4(M_1 M_2 + p_2)^2, \tag{5.1}$$

in the *Goryachev-Chaplygin* case

$$H = \frac{1}{2}(M_1^2 + M_2^2 + 4M_3^2) - 2p_1,$$

which has the additional integral

$$G = M_3(M_1^2 + M_2^2) + 2M_1 p_3. \tag{5.2}$$

This and more details can be found in e. g. [BBEIM].

Example. In the *Top Visualization* program a Kowalewski and a Goryachev-Chaplygin case is constructed from a quader with fixed point at the center of one of its faces. In the body frame (N, B, T) the center of mass lies on the axis spanned by T, hence i. e. in the plane spanned by B and T.

The quader with quader coordinates $(C_N, C_B, C_T) \in \mathbb{R}^3_+$ have the principal moments of inertia

$$I_1 = \frac{\mathcal{M}}{3}(C_B^2 + (2C_T)^2),\ I_2 = \frac{\mathcal{M}}{3}(C_N^2 + (2C_T)^2),\ I_3 = \frac{\mathcal{M}}{3}(C_N^2 + C_B^2),$$

which means for the Kowalewski case

$$2(C_B^2 + (2C_T)^2) = C_N^2 + (2C_T)^2 = C_N^2 + C_B^2$$

$$\Leftrightarrow C_T = \frac{1}{2}C_B, \quad C_N = \sqrt{3}C_B$$

and for the Goryachev-Chaplygin case

$$4(C_B^2 + (2C_T)^2) = C_N^2 + (2C_T)^2 = C_N^2 + C_B^2$$

[3] In the spinning top case there exist four integrable cases. The euler top has the fixed point at the center of mass, the Lagrange top is described in section 2.4 and the remaining two cases are described here.

[4] The Legendre transform of the Lagrangian, i. e. $H = T + U$, where T is the kinetic and U the potential energy.

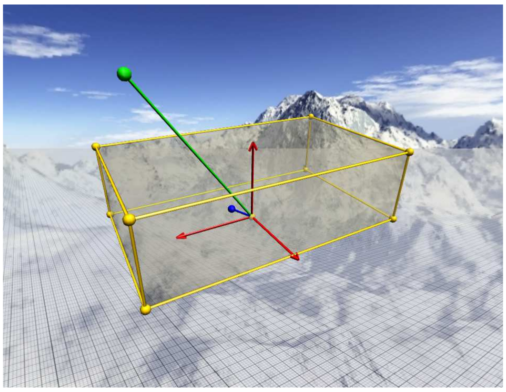

(a) A Kowalewski top.

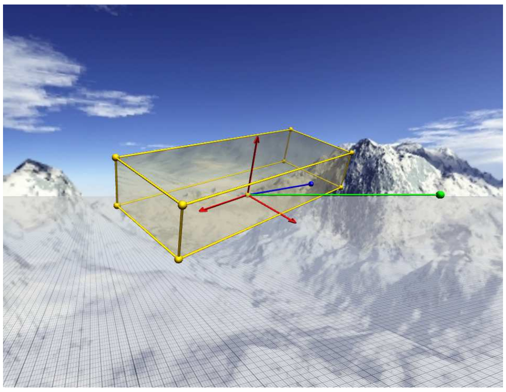

(b) A Goryachev-Chaplygin top.

Figure 5.4: Special integrable top cases.

$$\Leftrightarrow C_T = \frac{1}{2}C_B, \quad C_N = \sqrt{7}C_B$$

with the additional condition of $M_2 = 0$.

Hence, by clicking the checkboxes for those cases, just C_N and C_T are adjusted to C_B (and in the Goryachev-Chaplygin case additionally the vector of angular momentum). For examples see figures 5.4(a) and 5.4(b).

The corresponding integrals of motion 5.1 and 5.2 then appear next to the checkboxes and are recalculated every time a new motion step is performed. The occurring fluctuation is a measure of the exactness of the used discretization (which is in this case the *Extrap* method).

Example. An exemplary course of the error in the integral K can be seen in figure 5.5. Thereby the initial settings are the settings at startup of the *Top visualization* program, but with the quader adjusted to a Kowalewski top by clicking the *Kowalewski* checkbox. ε was 0.1 and the error was plotted over a period of 300 time units.

The integral G in the Goryachev-Chaplygin case shows a similar behaviour.

5.7 Elastic rods and the apex trace

The analogies stated in theorems 3.8 and 3.9 can be observed in the mode of arbitrary quaders. Then the tab *Rod & Apex trace* is availiable at which the elastic rod can be activated and configured. See figure 5.6.

5.7.1 Kirchhoffs analogy visualized

If the quader is a Lagrange top, Kirchhoffs analogy 3.9 is visualized as follows:

As described in section 3.5 the motion of the Lagrange top body frame is the frame of an isotropic elastic curve (or rod). Hence, by taking the body frame at every discrete time step, moving it by ε[5] to the direction of T (the third axis of the body frame, which points to the center of mass) and connecting the old and the new origin, one gets a discrete elastic rod.

But since that would move the frame away from the top, the origin is actually kept and instead all former points moved in negative T direction by ε. This way the same rod appears and stays close to the

[5] The current time step length.

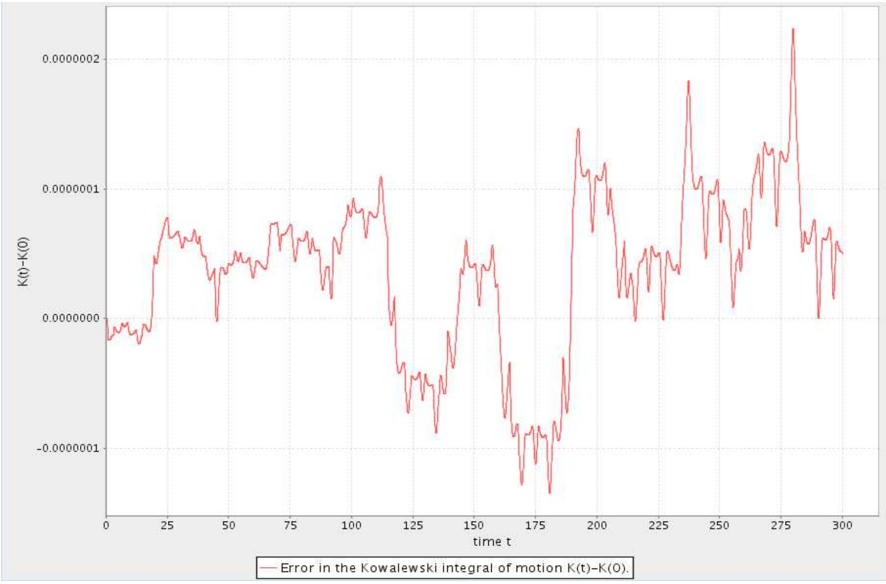

Figure 5.5: An exemplary error of the Kowalewski integral of motion $K(t) - K(0)$. A small error is a quality measure of the used discretization. The total value of K was in this settings approximately 0.5.

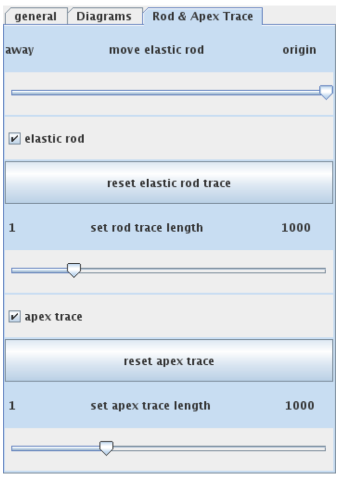

Figure 5.6: The *Rod & Apex Trace* tab of the *Top Visualization* panel.

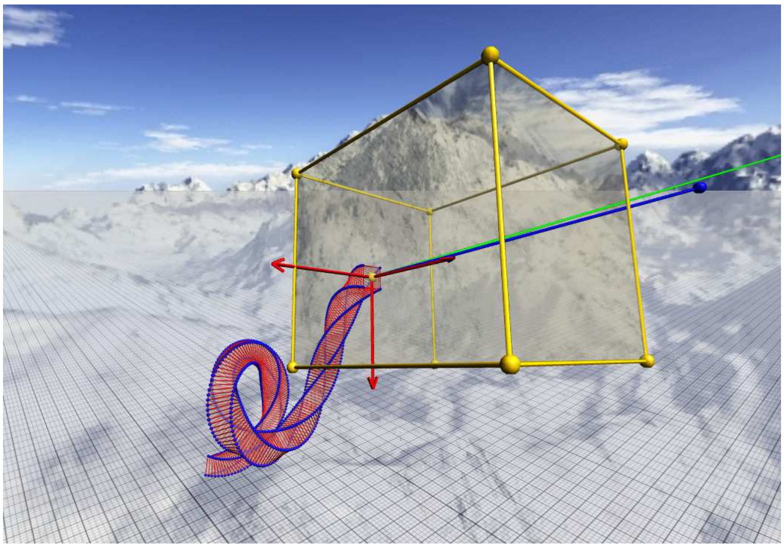

Figure 5.7: A Lagrange top with its corresponding isotropic elastic rod.

top. See figure 5.7. Also remark that the rod has a symmetric cross section, i. e. the bending energy is equal for all bending directions perpendicular to T, so that it really corresponds to a Lagrange top.

5.7.2 Analogy of tops and anisotropic elastic rods visualized

Analogy 3.8 between tops with gravity center on one of its principal axes and anisotropic elastic rods is visualized for the special cases of Kowalewski- and Goryachev-Chaplygin tops that appear when the corresponding checkboxes are activated, see figures 5.8(a) and 5.8(b).

In both of these cases the center of mass lies on a principal axis. This axis and a second one have identical moments of inertia; the third axis, in whose direction the quader is stretched out, has half respectively quarter the moment of inertia. Accordingly the bending energy of the elastic rod is also half/quarter, when rotating around this axis. This corresponds to a rod with half/quarter the thickness in the corresponding direction, see again 5.8(a) and 5.8(b).

5.7.3 The apex trace visualized

The apex trace is the trace of the intersection point of the symmetry axis of a Lagrange top and a sphere with the center at the fixed point. It shows two periodic motions, the nutation and precession, see e. g. [Arn]. Nutation is the periodic rise and fall of the apex trace, precession its azimuthal motion, see figure 5.9.

In the *Top Visualization* program one can show the apex trace when in the arbitrary quader mode, but the quader still has to be a Lagrange top (i. e. has coordinates (C_N, C_N, C_T)). Then, if not already activated, klick the *apex trace* checkbox in the *Rod & Apex trace* tab of the *Top Visualization panel*.

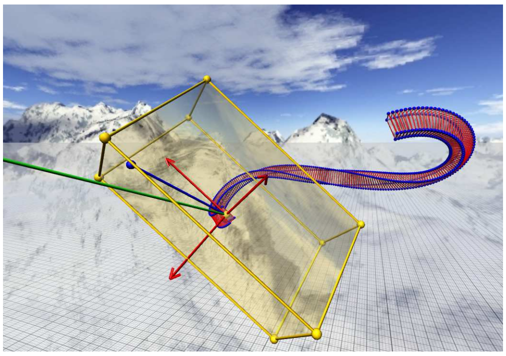

(a) Anisotropic elastic curve from Kowalewski top.

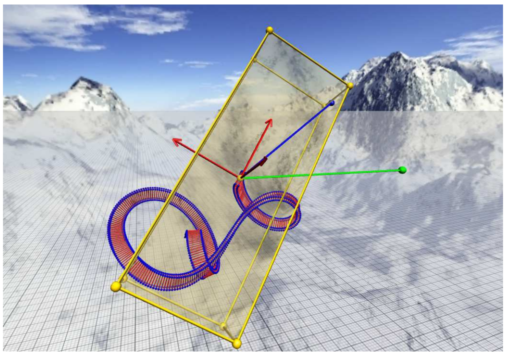

(b) Anisotropic elastic curve from Goryachev-Chaplygin top.

Figure 5.8: Anisotropic elastic curves.

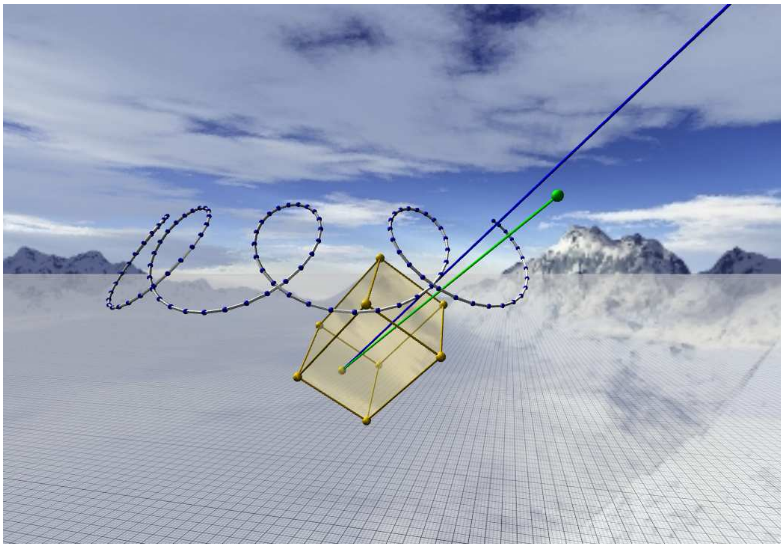

Figure 5.9: The apex trace of a Lagrange top, intersection of the symmetry axis and a sphere around the fixed point. The nutation is the periodic motion up and down, the precession left and right.

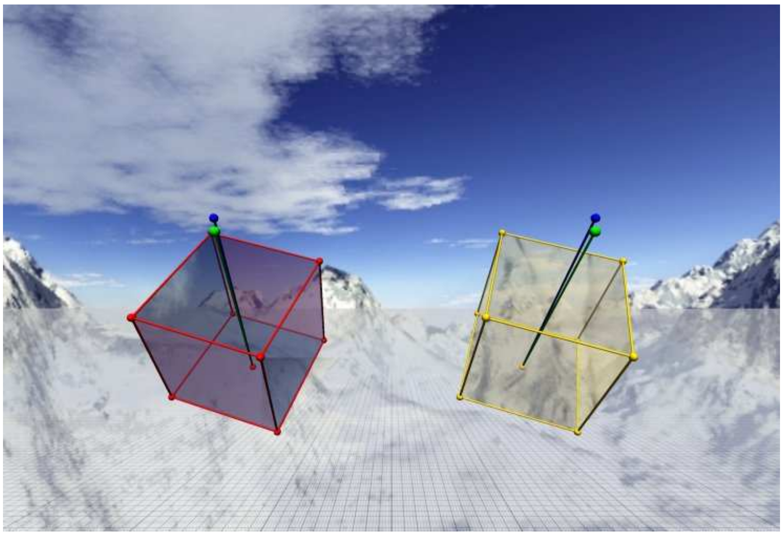

Figure 5.10: Quader with a duplicate of itself.

5.8 The Lagrange top mode

5.8.1 Same motion calculated with Bobenko-Suris discretization

By clicking the *Lagrange top* button in the *general* tab of the *Top Visualization panel* the present quader is resized to coordinates of the form (C_N, C_N, C_T) so that it gets a Lagrange top, see section 2.4.

Further a copy of the top is set into the scene at a certain distance[6] from the original one, see figure 5.10.

The motions of the two tops are calculated in different ways, the yellow one on the right side like an arbitrary quader with the *Extrap* discretization, see section 4.1.1, the red quader with the integrable discretization by A. I. Bobenko and Yu. B. Suris, see 4.2. The parameter used for the numerical discretization were $Atol = Rtol = 10^{-5}$ and the standard initial step size of $h = 0.1$.

This way the two discretizations can be directly compared. By setting the quader distance to zero with the *set quader distance* slider the positions can be compared during or after the motion. Unfortunately the "true" motion is not known so a qualitative assessment of the discretizations is not yet possible. But this can be achieved by introducing a second calculation step width ε_2, see later this section.

5.8.2 The stoptime

The timer stops when the actual time arrives at the stoptime. This is useful for repeated comparisons of motions with different discretizations or discrete time steps ε.

If in Lagrange top mode and the *eps2* checkbox is enabled, the stoptime is updated, everytime one of the ε is changed. The update makes sure the stoptime is a common multiple of the two different ε, so that after the stoptime is reached the different quader indeed have gone through the same time interval, see figure 5.12.

[6]The distance can be varied with the *set quader distance* slider in the *general* tab of the *Top Visualization panel*.

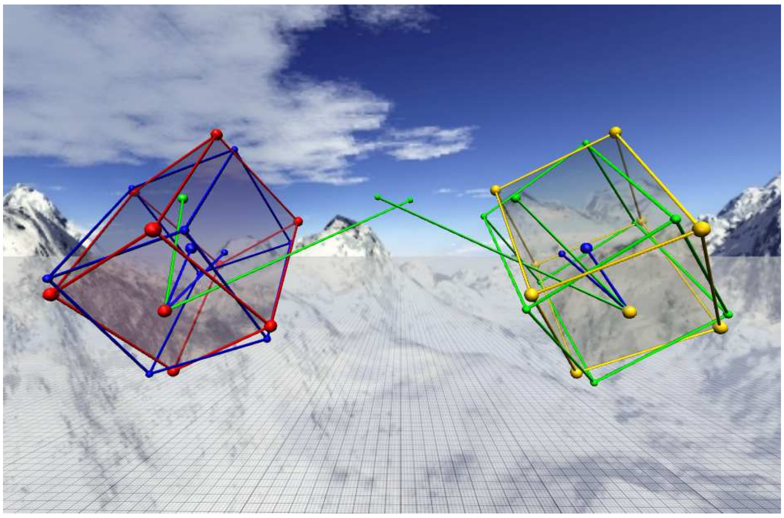

Figure 5.11: Langrange top mode with eps2 enabled. The two quader on the left side are calculated with the *Bobenko-Suris discretization*, the ones on the right side numerically. The two with thicker vertices were calculated with $\varepsilon_1 = 0.01$, so they resemble the continuous result. The quader with thinner vertices had $\varepsilon_2 = 0.2$. Their difference from the others is (approximately) the error that occurred in discretizing the tops path. The vectors of angular momentum are green, vectors of angular velocity blue. Vectors with thicker vertices correspond to the quader with thicker vertices.

5.8.3 Quader distance

In *Lagrange top* mode, the distance between the quader can be changed. This way it is easier to distinct or compare the up to four different quader.

5.8.4 Epsilon2

In Lagrange top mode, one can compare the two discretizations among each other, but not yet assess their quality. This can be achieved with a second discretization step length parameter ε_2. Choose e. g. ε_1 very small and calculate the motion of the quader the result will be close to the continuous one. Computing at the same time the motion of the quader with a larger ε_2, but identical initial settings, one gets the discrete results and can compare them to the "continuous" ones. See figure 5.11.

Summarization of the different quader:

color	position	vertices	discretization	ε	corresponding vectors
red	left	thick	*Bobenko-Suris*	ε_1	left side, thick vertices
blue	left	thin	*Bobenko-Suris*	ε_2	left side, thin vertices
yellow	right	thick	*Extrap*	ε_1	right side, thick vertices
green	right	thin	*Extrap*	ε_2	right side, thin vertices

When the eps2 checkbox is enabled, two additional tabs are added which show the integrals of motion and diagrams with statistics of the different quader. For details see section 5.9 and chapter 6.

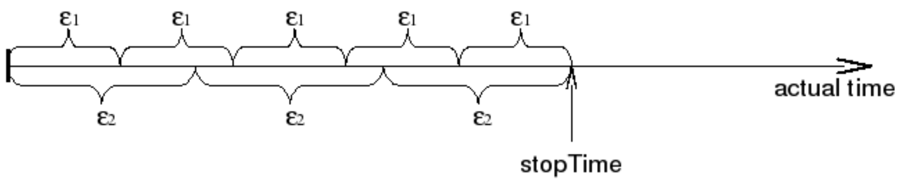

Figure 5.12: Functionality of the timer. Every time a multiple of ε_1 respectively ε_2 is reached, a motion step of the corresponding quader is calculated. The stopTime is (automatically updated to) a common multiple of ε_1 and ε_2. The actual time displayed in the *Top Visualization* program is only updated when a multiple of ε_1 is reached.

5.8.5 The timer

In order to intuitively visualize motions of quader whose paths were discretized with two different discretization step length parameters ε, the *Top Visualization* program uses a timer. Its functionality is shown in figure 5.12.

5.9 Comparing discretizations, Eps2Tab and Diagrams tab

This section shows some possibilities to compare the numerical discretization of the Lagrange tops path to the *Bobenko-Suris* one. Therefore the *Lagrange top mode* has to be activated. Also, to have a possibility to compare the discrete paths to the "nearly continuous" ones, ε_2 should be enabled and (preferrably) ε_1 set very small.

Again the summarization of the different quader:

color	position	vertices	discretization	ε	corresponding vectors
red	left	thick	*Bobenko-Suris*	ε_1	left side, thick vertices
blue	left	thin	*Bobenko-Suris*	ε_2	left side, thin vertices
yellow	right	thick	*Extrap*	ε_1	right side, thick vertices
green	right	thin	*Extrap*	ε_2	right side, thin vertices

5.9.1 Visual comparison

The simplest way to compare the discretizations is to just calculate the paths of the four tops and see whether the discrete paths are close to the "continuous" paths. I. e. , if ε_1 was chosen small, the numerical discretization is good if the green quader is close to the yellow one, the *Bobenko-Suris discretization* is good if the blue quader is close to the red one.

An example for that can be seen in section 6.1.2.

5.9.2 Error in the body frame

The *Top Visualization* program provides an analytic measure of the correctness of the quader position, its body frame. It is described in section 6.1.3, calculated and visualized in the lower diagram in the *Diagrams* tab, see e. g. figure 5.14.

Again the results of an exemplary experiment are given in section 6.1.3.

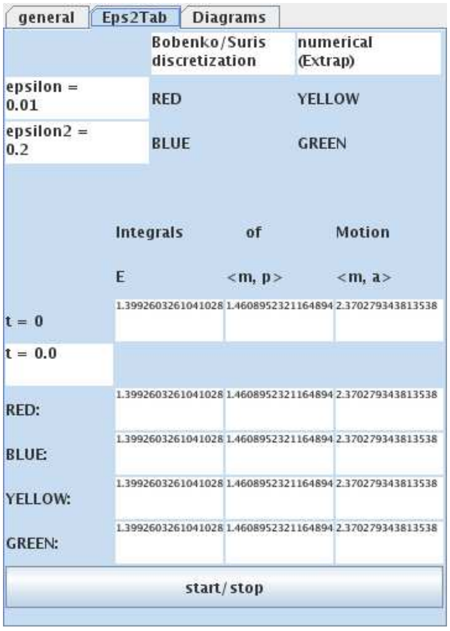

Figure 5.13: The values $\langle m, p\rangle$, $\langle m, a\rangle$ and $E = \frac{1}{2}\langle m, \omega\rangle + \mathcal{M}\langle p, a\rangle$ are calculated for the four different quader and displayed in the *Eps2Tab*. The closer they stay to the initial value at $t = 0$, the better the discretization.

5.9.3 Integrals of motion

With the notations

m	vector of angular momentum
ω	vector of angular velocity
p	gravity vector, pointing in positive e_3-direction
a	vector pointing to the center of mass
$\mathcal{M}$	mass of the top

the Lagrange top has the three integrals of motion $\langle m, p\rangle$, $\langle m, a\rangle$ and $E = \frac{1}{2}\langle m, \omega\rangle + \mathcal{M}\langle p, a\rangle$. I. e. in the continuous motion they stay constant. Therefore it is a quality measure for a discretization if these values indeed stay constant at the discrete path.

The three values are calculated for all four quader and displayed in the *Eps2Tab*, see figure 5.13. The closer they stay to the initial value the better the discretization.

Further the difference $E - E_0$ of the top energy to its initial value is visualized in the upper diagram in the "Diagrams" tab. The values for the four different quader can be observed seperately, see e. g. figure 5.14.

For exemplary evaluations, see section 6.1.4.

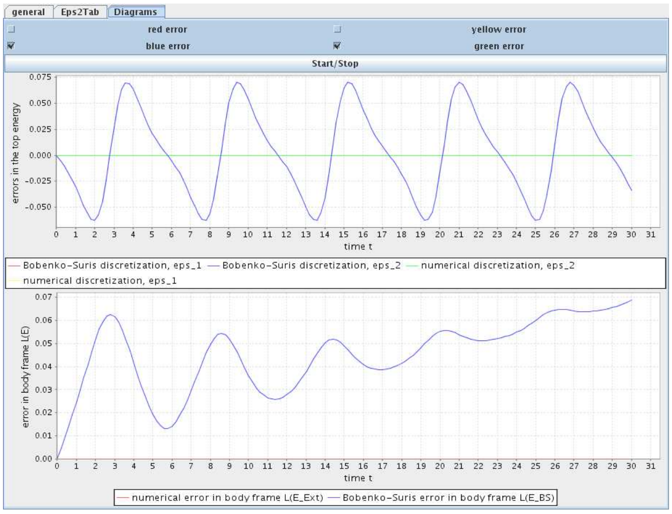

Figure 5.14: The upper diagrams shows the error in the energy of the different discretizations. The lower one shows the measured error in the body frame. The errors can be shown seperatelyby activating the corresponding checkboxes. The errors in the lower diagram only make sense for the blue and the green quader and if ε_1 was chosen small.

Chapter 6

Results

6.1 Comparison of the *Bobenko-Suris discretization* to the *Extrap* method

In this section the *Bobenko-Suris discretization* of the path of a Lagrange top is compared to a numerical discretization, i. e. the *Extrap* method of solving ordinary differential equations. Therefore the motion of the top was calculated with the two different discretization methods and with two different ε. The initial settings were chosen arbitrary. One can repeat the experiments in the *Top Visualization* program. At startup the quader have the same settings used for the experiment in this section.

6.1.1 Settings

In the experiments there are four different quader. See figure 6.1 for an example of the quader after they already moved for 300 time units.

They all had the same position, the same size, density, vector of angular momentum and gravity vector at time zero.

For better distinction, they lie in two coordinate systems with shifted origin. The two quader on the left side, the red and the blue one, had their motion calculated with the *Bobenko-Suris discretization*, the two on the right side, yellow and green, numerically.

On each side there is one quader with thicker vertices and one with thinner ones. The quader with thick vertices, red on the left side and yellow on the right side, had their motion calculated with the parameter ε_1. The quader with thin vertices with parameter ε_2.

The experiment took place in the *Lagrange top mode* with a small ε_1, so that the motions of the red and yellow quader, both with thick vertices, resemble the continuous motion.

The used numerical method is *Extrap* implemented in the package [TBb], see section 4.1.1, with accuracy parameters of $Atol = Rtol = 10^{-5}$ (chosen experimentally to balance calculation time and accuracy) and the standard initial step size of $h = 0.1$. This method showed a better performance than e. g. the *Runge-Kutta* method of solving ordinary differential equations.

The data used for the experiment is:

ε_1	0.01
ε_2	0.2
gravity	1
quader coordinates	$(0.8,\ 0.8,\ 1)$
vector of angular momentum	$(0.172,\ -1.862,\ 1.46)$

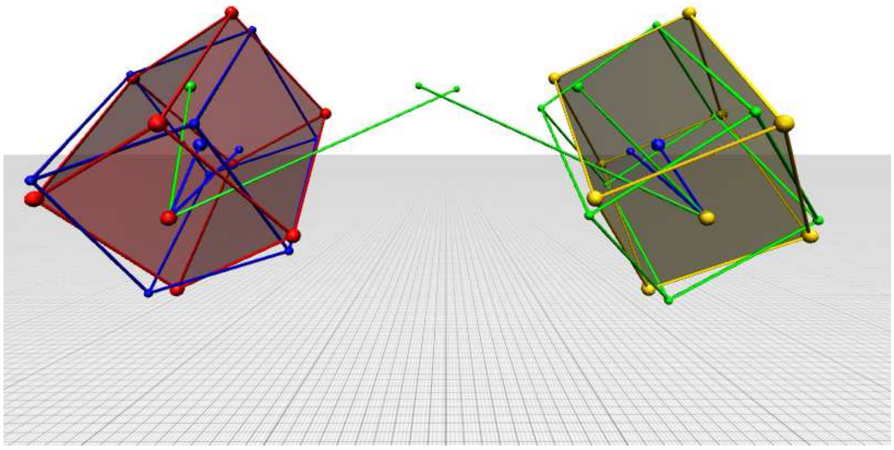

Figure 6.1: Four quader which had identical positions at the beginning and whose motions were calculated in four different ways for 300 time units. The two on the left side were calculated with the *Bobenko-Suris discretization*, the two on the right side numerically. Quader with thick vertices had parameter $\varepsilon_1 = 0.01$, the ones with thin vertices $\varepsilon_2 = 0.2$. The long green vectors are the corresponding vectors of angular momentum, the shorter blue vectors are the vectors of angular velocity.

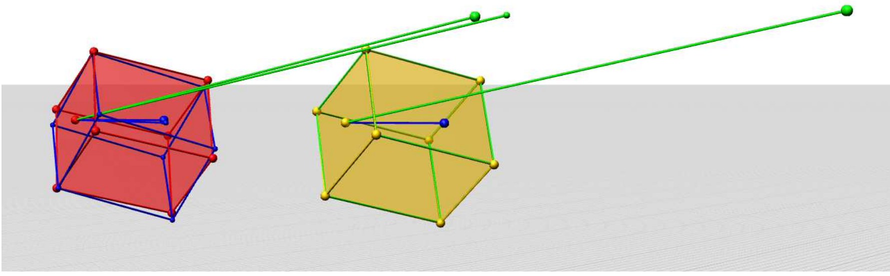

Figure 6.2: Position of the quader after 50 time units. The numerical discretiations shows no visible errors yet.

Finally, there are different vectors visible in the scene. Each quader has its vector of angular momentum (green and long in figure 6.1) and its vector of angular velocity (blue and short). The vectors with thicker vertices correspond to the quader with thicker vertices. This way one can compare the paths of the vectors for different calculation step lengths ε.

Summarization of the different quader:

color	position	vertices	discretization	ε	corresponding vectors
red	left	thick	*Bobenko-Suris*	0.01	left side, thick vertices
blue	left	thin	*Bobenko-Suris*	0.2	left side, thin vertices
yellow	right	thick	*Extrap*	0.01	right side, thick vertices
green	right	thin	*Extrap*	0.2	right side, thin vertices

6.1.2 Visual results

After 50 time units the quader are in the positions seen in figure 6.2, after 300 time units see figure 6.3 and after 600 time units see figure 6.4.

It can be seen that in the beginning the body frame calculated with the *Bobenko-Suris discretization* (blue, left side with thin vertices) differs more from its "continuous" position (red, left side with thick vertices) than the one calculated with *Extrap* (green, right side with thin vertices) is to its "continuous" counterpart (yellow, right side with thick vertices). But after longer time periods this changes to the vice versae. This will be analyzed further later this chapter.

6.1.3 Error in the body frame

In this section the error in the body frame is investigated analytically.

Denote therefore

$$\Phi_{red},\ \Phi_{blue},\ \Phi_{yellow},\ \Phi_{green} \in SU(2)$$

the rotation from the rest frame to the body frame of the corresponding quader. For a recall of the used algebra see section 3.2.

Then

$$SU(2) \ni E_{BS} := \Phi_{blue}\Phi_{red}^{-1}$$

is the rotation from the "continuous" red quader body frame to the blue quader body frame. Hence E_{BS} is the error in the body frame that occurred using a high ε_2 in the *Bobenko-Suris discretization*.

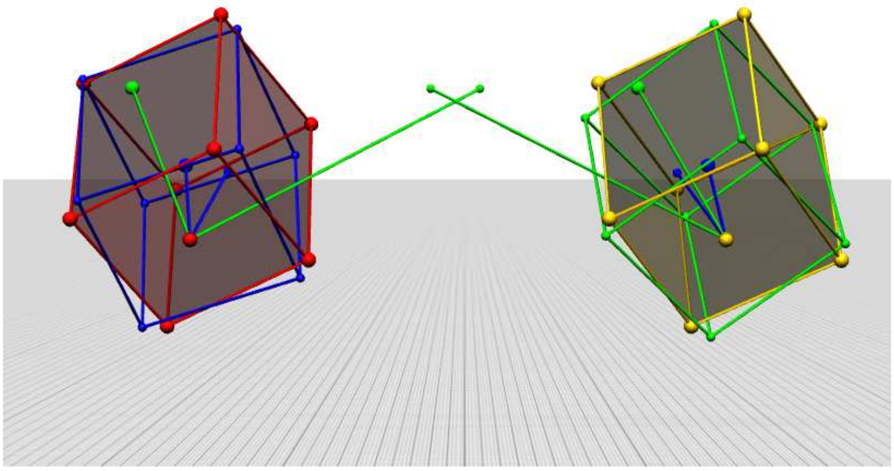

Figure 6.3: Position of the quader after 300 time units. Both discretizations show more or less comparable errors.

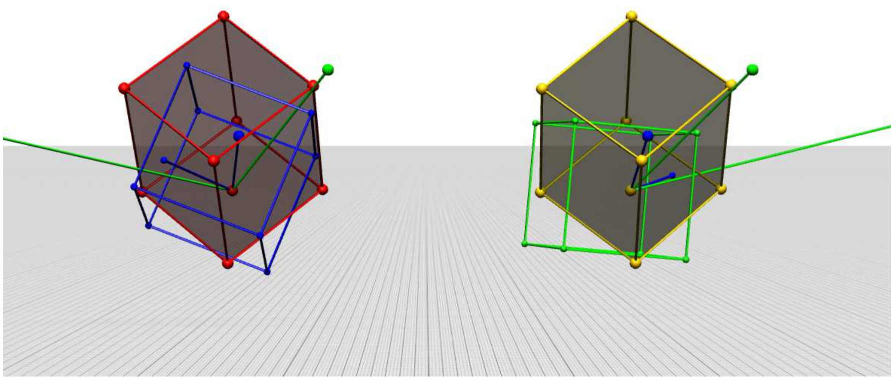

Figure 6.4: Position of the quader after 600 time units. Both discretizations show big errors, whereas the integrable one is still somewhat closer to the "continuous" result.

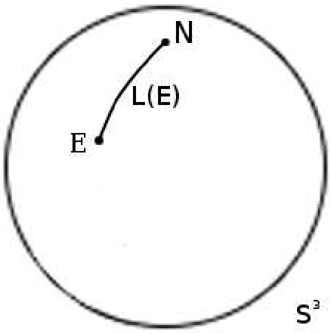

Figure 6.5: L(E), the length of the geodesic from E to N, as measure of the error in the body frame E.

Similarly let

$$SU(2) \ni E_{Ext} := \Phi_{green}\Phi_{yellow}^{-1}$$

be the error in the body frame that occurred using a high ε_2 in the *Extrap* discretization.

To make these error matrices comparable, consider the following observations. An arbitrary rotation $E \in SU(2)$ can be written as

$$\begin{aligned} E &= \begin{pmatrix} a & b \\ -\bar{b} & \bar{a} \end{pmatrix} \quad a,\, b \in \mathbb{C} \\ &= \begin{pmatrix} a_1 + ia_2 & b_1 + ib_2 \\ -b_1 + ib_2 & a_1 - ia_2 \end{pmatrix} \quad a_i,\, b_i \in \mathbb{R} \end{aligned}$$

with

$$\begin{aligned} det(E) &= 1 \\ \Leftrightarrow \quad a_1^2 + a_2^2 + b_1^2 + b_2^2 &= 1. \end{aligned}$$

Therefore E_{BS} and E_{Ext} correspond to vectors in S^3. The identity matrix, which corresponds to "no error in the body frame", has $a_1 = 1$ and $a_2 = b_1 = b_2 = 0$, which is the north pole of the unit sphere S^3. Hence the error in the body frame is the smaller the closer its corresponding vector in S^3 lies to the north pole. See figure 6.5.

As a measure of the errors in the rest frame one can use the length of the geodesic from an error matrix $E \in S^3$ to the north pole of S^3.

$$\begin{aligned} \widetilde{L} :\ S^3 &\longmapsto \mathbb{R}^+ \\ E &\longrightarrow \widetilde{L}(E) = \{\text{length of geodesic from } E \text{ to } N\} \end{aligned}$$

Since the geodesics on S^3 are great circles and the length of a segment between E and N is the included angle, one gets

$$\widetilde{L}(E) := \measuredangle(E, N) = \arccos\frac{\langle E, N\rangle}{\|E\| \cdot \|N\|} = \arccos(a_1) \in [0, \pi].$$

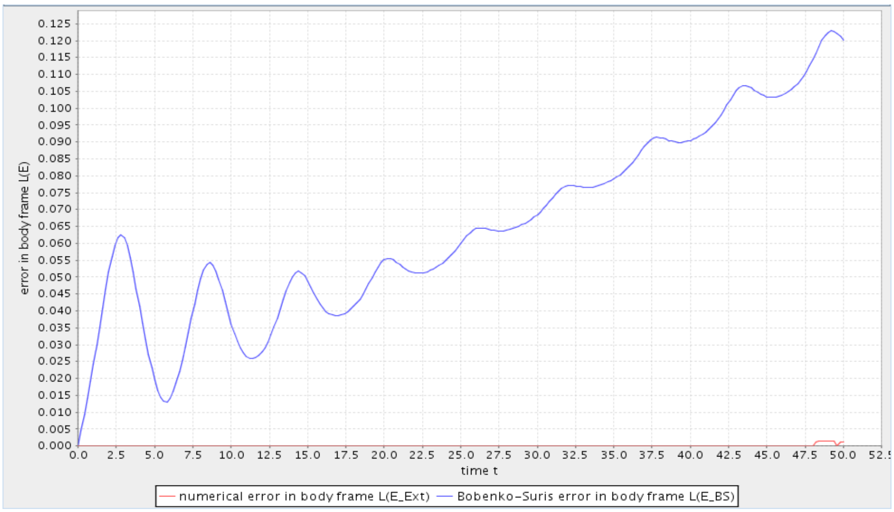

Figure 6.6: Errors in the body frame for $\varepsilon = 0.2$ after 50 time units. The error in the numerical discretization is neglible compared to the one in the integrable discretization.

But since by theorem 3.4 the error matrices in $SU(2)$ are only unique up to $\Phi \mapsto \pm\Phi$ and in the implementation it cannot be determined, which one is obtained, in the *Top Visualization* program $\|a_1\|$ is used instead of a_1. Hence

$$L(E) := \arccos(\|a_1\|) \in [0, \frac{\pi}{2}]$$

is used.

$L(E_{BS})$ and $L(E_{Ext})$ are calculated and visualized in diagrams, see figures 6.6, 6.7 and 6.8.

In both discretizations there seems to be a fluctuation and a trend, though in the *Bobenko-Suris discretization* the trend seems almost linear, whereas in the numerical one it is more or less quadratic.

6.1.4 Error in the integrals of motion

With the notations

m	vector of angular momentum
ω	vector of angular velocity
p	gravity vector, pointing in positive e_3-direction
a	vector pointing to the center of mass
$\mathcal{M}$	mass of the top

the Lagrange top has the three integrals of motion $\langle m, p\rangle$, $\langle m, a\rangle$ and $E = \frac{1}{2}\langle m, \omega\rangle + \mathcal{M}\langle p, a\rangle$.

In the experiment $\langle m, p\rangle$ stays constant in both discretizations and for all ε.

The behaviour of $\langle m, a\rangle$ for $\varepsilon = 0.2$ can be seen in figure 6.9. The seen value is the actual $\langle m, a\rangle$ minus the one at $t = 0$. The integrable discretization yields as expected no error since it is an integral of motion of the *Bobenko-Suris discretization*, see [BS00]. In the numerical discretization the error small but it is constantly increasing.

Another quality measure for the different discretizations of the tops path is the error in the energy of the top $E - E_0$, E_0 being the energy at $t = 0$. The error in the *Bobenko-Suris discretization* shows a periodic behaviour proportional to ε, see figure 6.10.

For a comparison to the error in the energy in the numerical discretization see figure 6.11. The error in the numerical discretization increases fast after longer time periods, while the error in the integrable

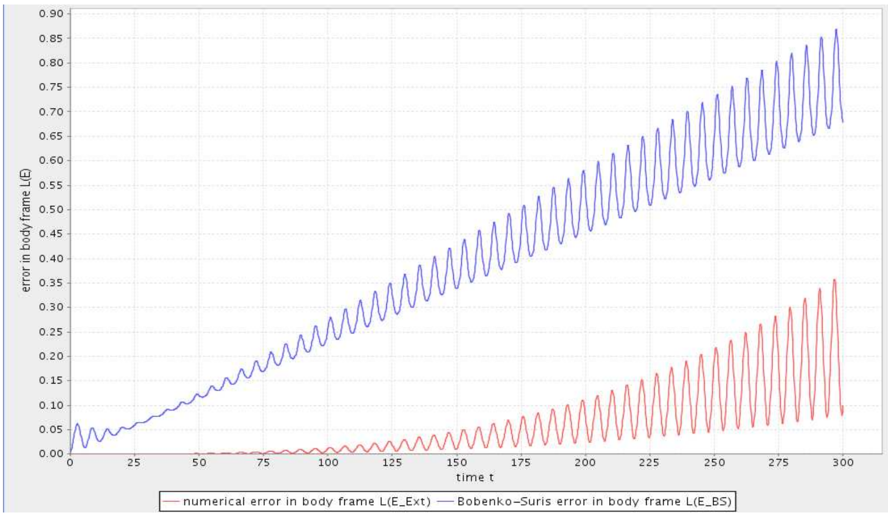

Figure 6.7: Errors in the body frame for $\varepsilon = 0.2$ after 300 time units. The numerical error is lower but already has a trend comparable to the *Bodendo-Suris* one.

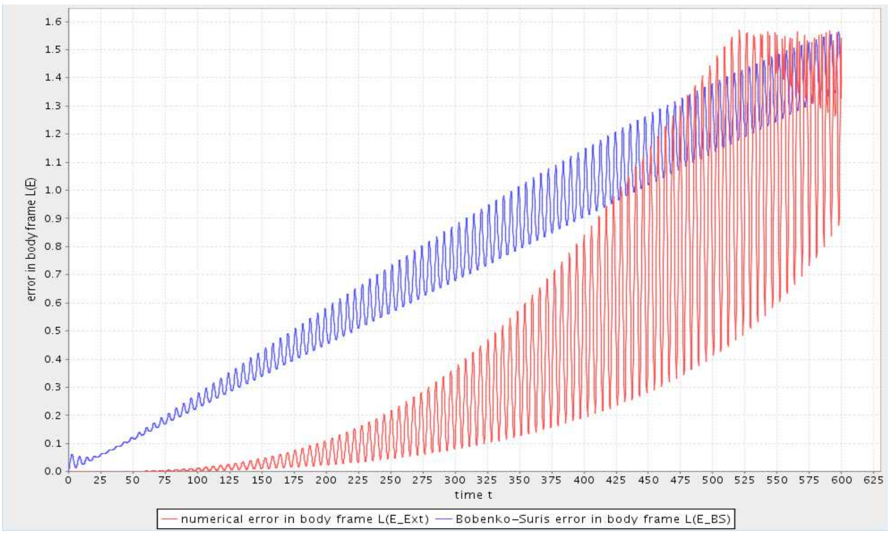

Figure 6.8: Errors in the body frame for $\varepsilon = 0.2$ after 600 time units. Both have reached the maximal possible error of $L \in [0, \frac{\pi}{2}]$, but the trend of the numerical error is much higher.

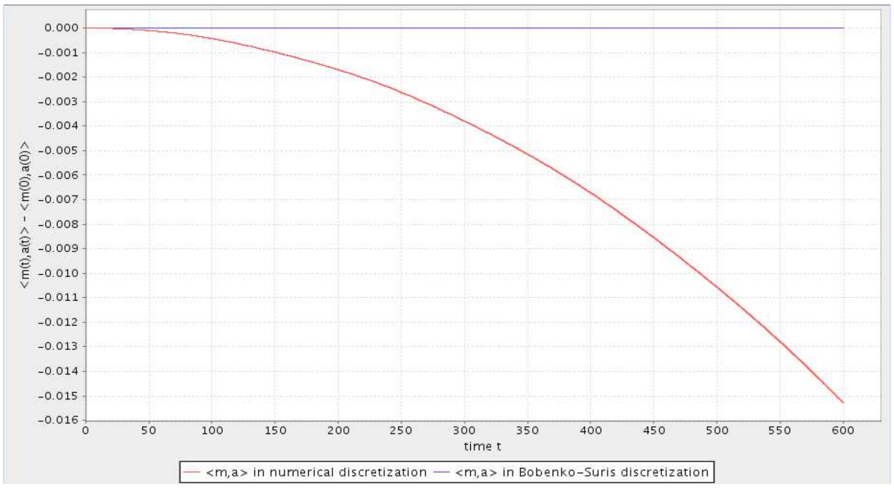

Figure 6.9: Behavior of $\langle m, a\rangle - \langle m, a\rangle\,|_{t=0}$ for $\varepsilon = 0.2$ in the first 600 time units. In the *Bobenko-Suris discretization* it is constant, in the numerical discretization the error is small but steadily increases.

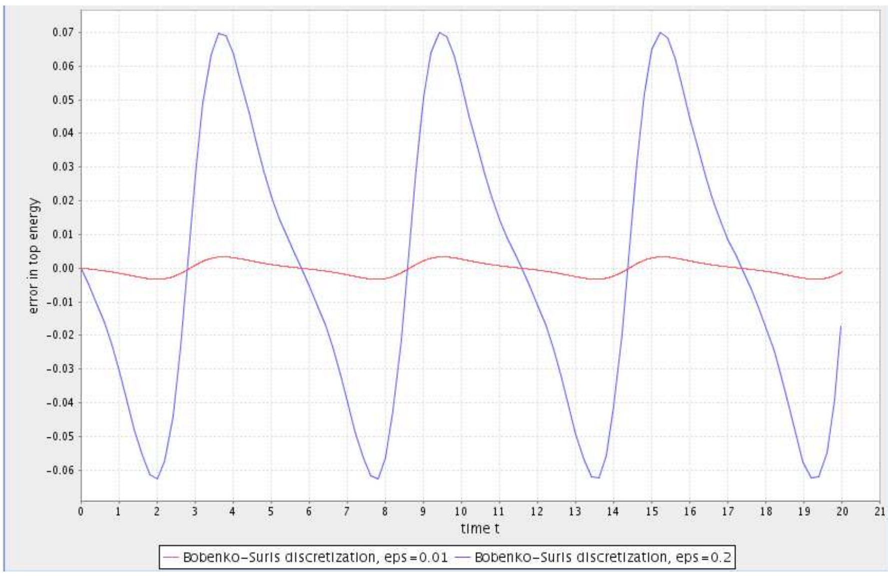

Figure 6.10: Error in energy $E - E_0$ in *Bobenko-Suris discretization* for $\varepsilon_1 = 0.01$ and $\varepsilon_2 = 0.2$. The error is a periodic oszillation proportional to ε.

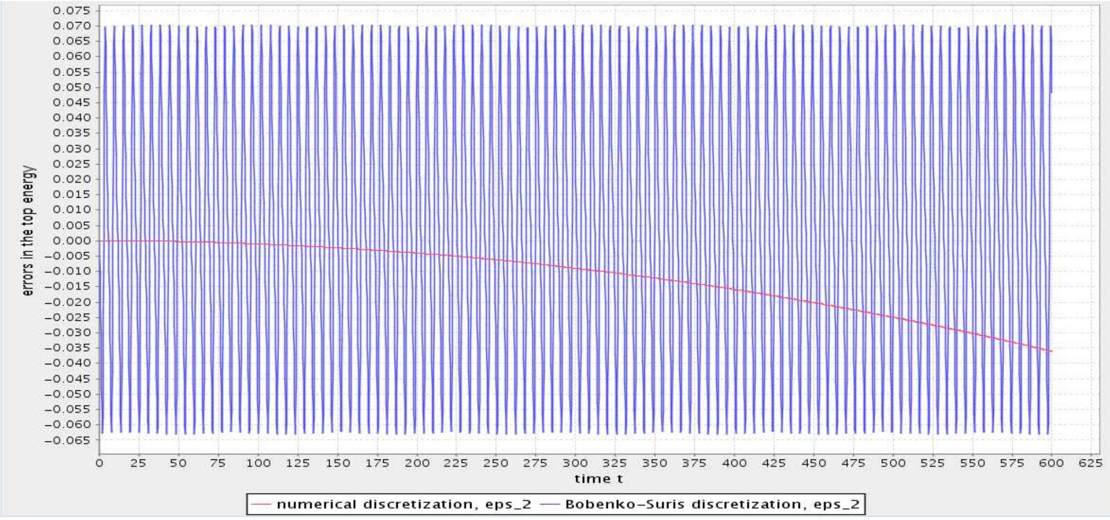

Figure 6.11: Error in energy $E - E_0$ in both discretizations for $\varepsilon_2 = 0.2$. In the beginning the numerical error is very small. Later it increases fast while the integrable error stays oscillating.

case keeps oscillating constantly.

Reason for this oscillation is that this integrable discretization has the discrete integral of motion

$$H_\varepsilon = \frac{1}{2}\langle \tilde{m}, \tilde{m}\rangle + \langle \tilde{p}, \tilde{a}\rangle + \frac{\varepsilon}{2}\langle \tilde{a} \times \tilde{m}, \tilde{p}\rangle\,,$$

see [BS00]. Thereby the used values are the coordinates wrt the scaled coordinate system, see section 4.2.1. The first two terms in H_ε are the energy of the top in these coordinates. The value H_ε indeed stays constant in the experiment which implies that the error in the energy in the *Bobenko-Suris discretization* is the additional term $\frac{\varepsilon}{2}\langle \tilde{a} \times \tilde{m}, \tilde{p}\rangle$.

6.1.5 Further Observations

In figure 6.12 the error in the energy of the top is opposed to the error in the body frame in the *Bobenko-Suris discretization* for $\varepsilon = 0.2$. One can observe a correlation between the oscillating error in energy caused by the term $\frac{\varepsilon}{2}\langle \tilde{a} \times \tilde{m}, \tilde{p}\rangle$ and the oscillating part of the error in the body frame.

Moreover, the term $\frac{\varepsilon}{2}\langle \tilde{a} \times \tilde{m}, \tilde{p}\rangle$ plays a central role for the quality of the integrable discretization. E. g. using settings that increase this term, like a vector of angular momentum m that is longer or more perpendicular to the center of mass a, or a higher gravity constant g and hence a longer gravity vector p, the exactness of the discrete motion decreases. See figures 6.13 and 6.14 for the results of a motion with initial settings as above except of a gravity constant of $g = 10$ and a vector of angular momentum $m = (5, 0, 0)$.

As expected the results of the integrable discretization are very bad.

6.2 Comparison of the *Bobenko-Suris discretization* to *Extrap* comprising execution time

The first experiment is in so far unfair, that the numerical discretization is a multi-step method and works effectively with a (variable but) smaller discretization step length parameter than the integrable discretiza-

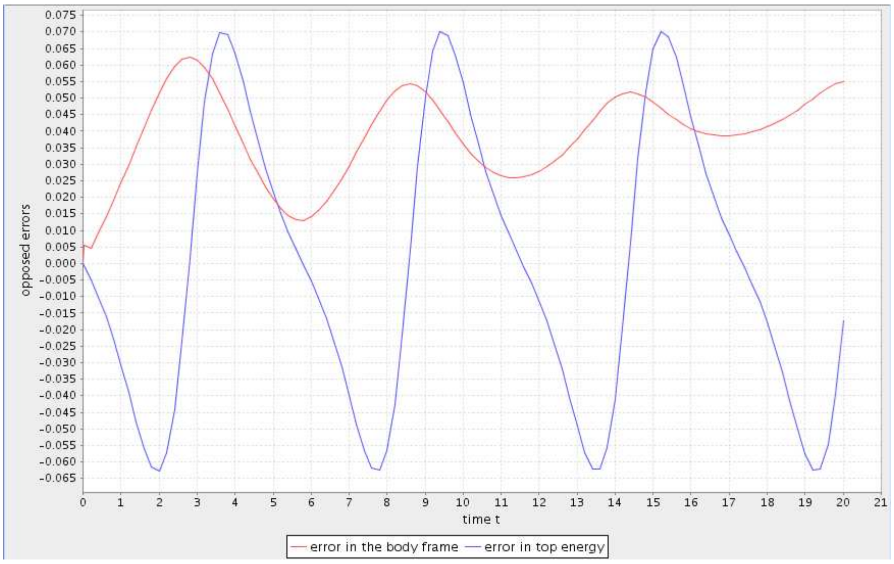

Figure 6.12: Error in energy $E - E_0$ opposed to the error in the body frame $L(E_{BS})$ in the *Bobenko-Suris discretization* for $\varepsilon = 0.2$. One can observe a correlation between the (oscillating) error in the energy and the oscillating part of the error in the body frame.

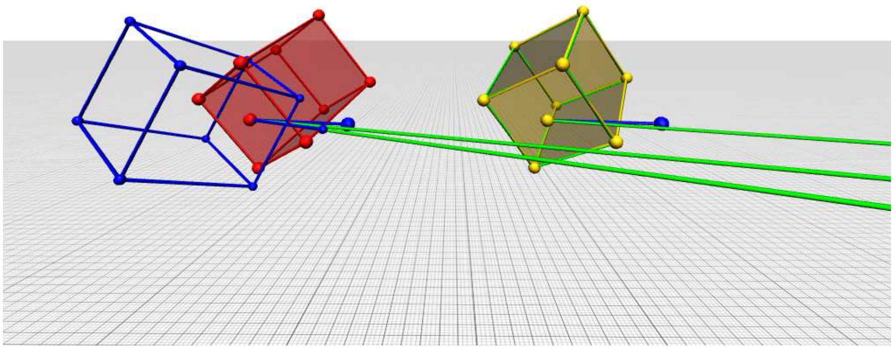

Figure 6.13: Visual result of an experiment with a high error term $\frac{\varepsilon}{2} \langle \tilde{a} \times \tilde{m}, \tilde{p} \rangle$ after $t = 20$ time units. The position of the quader calculated with the integrable discretization is already very wrong after that short time period.

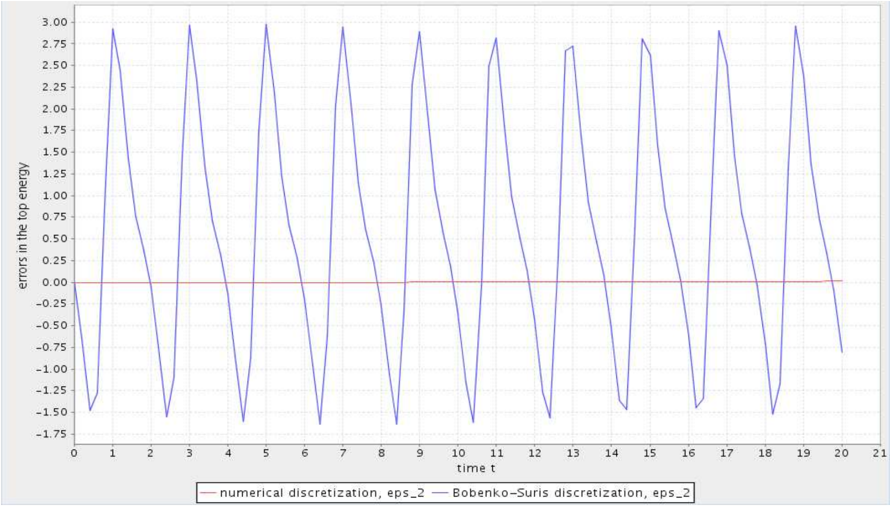

Figure 6.14: Error in the energy in an experiment with a high error term $\frac{\varepsilon}{2}\langle\tilde{a}\times\tilde{m},\tilde{p}\rangle$ after $t = 20$ time units. The oscillating error in the energy of the integrable discretization is of very high magnitude.

tion. Further the numerical method needs more execution time.

When asking the question, which discretization is more suitable for practical purposes, one might want to compare their performance for a given amount of computational capacity. This is done in an example in this section.

Unfortunately this was only possible with modified source code of the *Top Visualization* program and can therefore not be repeated like the first experiment.

6.2.1 Settings

The initial position of the quader, vectors of angular velocity and momentum and gravity vector are the same as in the first experiment.

In order to compare the discretizations for a fixed given execution time, only the discretization step length parameter and the error tolerances $Atol$ and $Rtol$, see section 4.1.1, are changed. I. e. the used values are:

$\varepsilon_1 = 0.01$	the parameter for the "continuous" motion, to assess the discrete ones.
$\varepsilon_2 = 5$	the interval length, for which the discretizations will be assigned a fixed amount of execution time to compute a best possible result. The quaders path is continuously calculated after every 5 time unit steps, so that it can be determined up to arbitrary time points $5n,\ n \in \mathbb{N}$, and the results can be compared after every 5 time units.
$m = 166$	the number of intervals $[5n,\ 5(n+1)],\ n \in \mathbb{N}$, is seperated into for the *Bobenko-Suris* discretization. This yields an effective discretization step length parameter of 0.03.
$Atol = Rtol = 2 \cdot 10^{-8}$	the error tolerances for the *Extrap* method, see section 4.1.1.
$h = 1.5$	the initial step size at the beginning of each interval $[5n,\ 5(n+1)]$, $n \in \mathbb{N}$. Changing this step size within this order of magnitude showed practically no change, since it is quickly adjusted by the *Extrap* method and since initially too high h are rejected without much loss of calculation time.

These values were determined experimentally to satisfy the following conditions:

1. Both discretization methods use the same amount of execution time. With these settings they needed an average of 0.8 milliseconds to calculate the next quader position after further 5 time units. The calculations were done in Java™ on a Linux system with an Intel® Core™ 2 Duo CPU with 2×2.00GHz.

2. $\varepsilon_2 = 5$ and $Atol = Rtol = 2 \cdot 10^{-8}$ were chosen in such a way, that the *Extrap* method could use its property of step size control effectively. For the interval $[5n, 5(n+1)],\ n \in \mathbb{N}$, an average of 7 steps are calculated.

3. The for the *Bobenko-Suris* discretization effectively used discretization step length parameter 0.03 is still comparable to the parameter 0.01 used for the "continuous" result.

These settings yielded the following results.

6.2.2 Visual results

The visual results of the experiment can be seen in figures 6.15, 6.16, 6.17 and 6.18.

It can be observed that in the beginning the numerical discretization yields better results, but its transported errors accumulate in time and let it yield weaker results after longer time periods.

6.2.3 Error in the body frame

The errors in the body frame, see section 6.1.3, can be seen in figures 6.19, 6.20 and 6.21.

6.2.4 Error in the energy

The errors in the energy of the quader can be seen in figures 6.22 and 6.23.

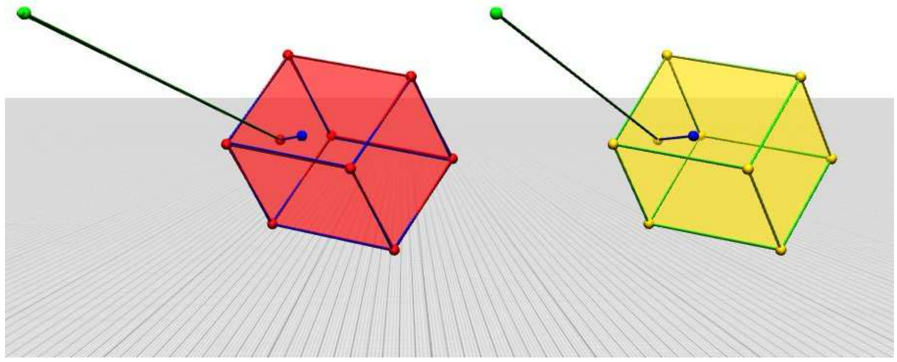

Figure 6.15: Position of the four quader after $t = 200$ time units in the experiment comprising execution time. There are almost no errors recognizable.

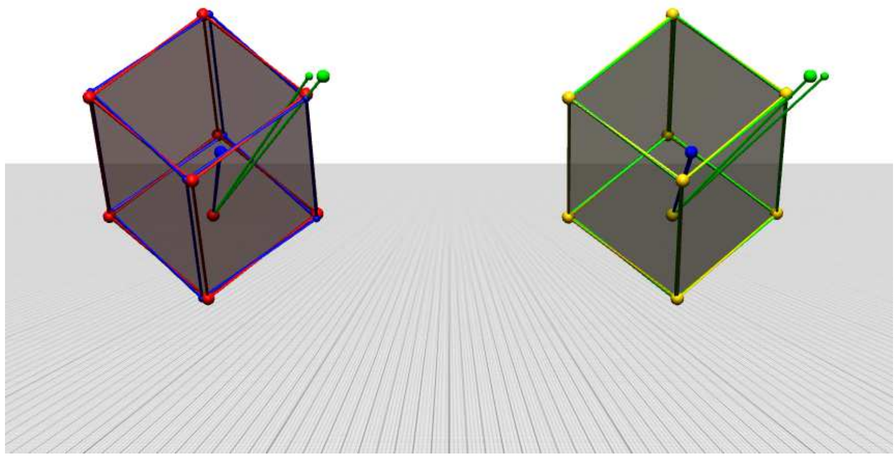

Figure 6.16: Position of the four quader after $t = 600$ time units in the experiment comprising execution time. Both discretizations start to show errors, whereas the *Bobenko-Suris* discretization has a little higher error in the quader position.

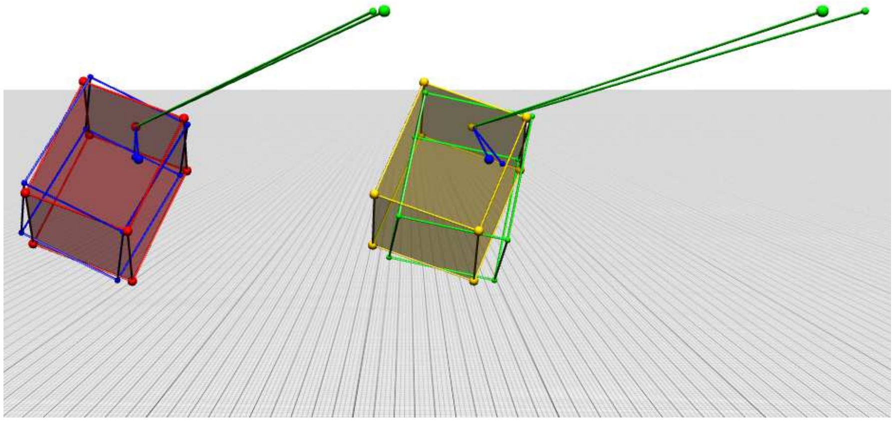

Figure 6.17: Position of the four quader after $t = 1000$ time units in the experiment comprising execution time. The errors in the numerical discretization increase faster.

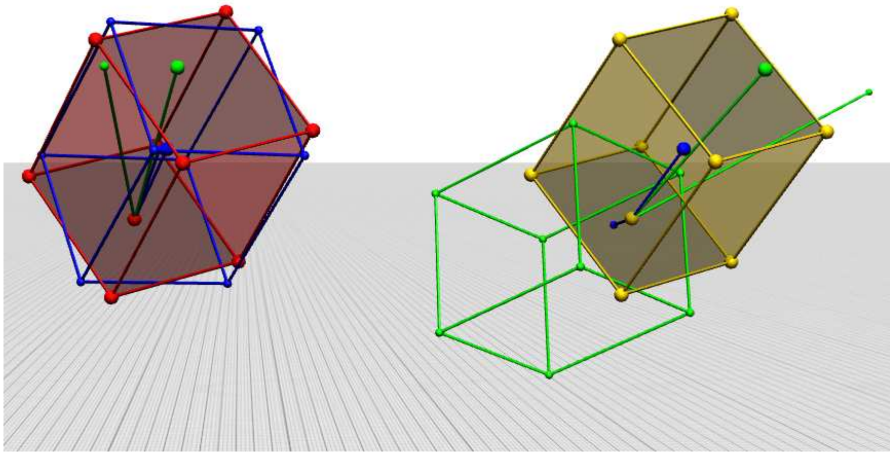

Figure 6.18: Position of the four quader after $t = 3200$ time units in the experiment comprising execution time. The errors in the integrable discretization are still somewhat acceptable, while the errors in the numerical one have gotten very big.

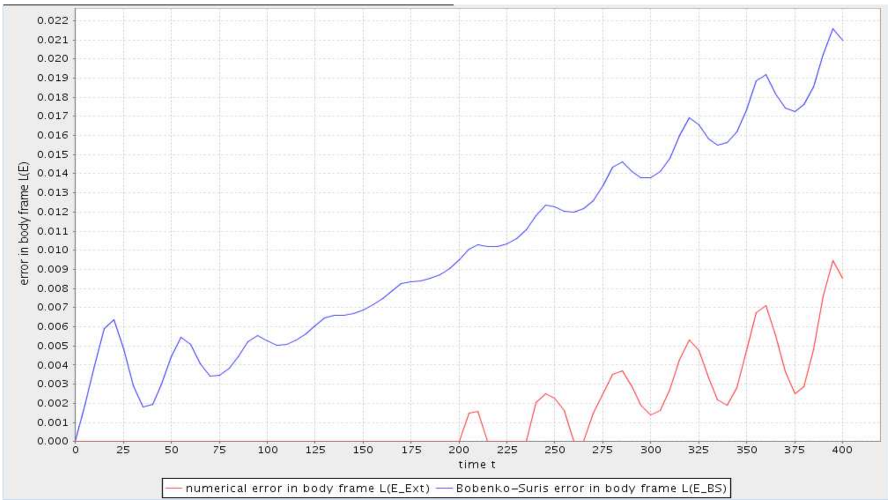

Figure 6.19: Errors in the body frame after $t = 400$ time units in the experiment comprising execution time. The error in the *Bobenko-Suris* discretization is higher. The numerical error is neglible in the beginning and low after 200 to 400 time units.

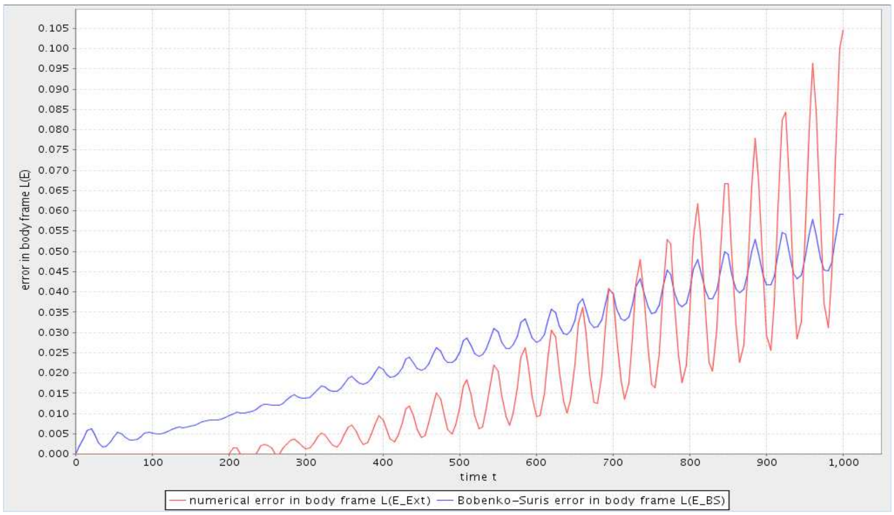

Figure 6.20: Errors in the body frame after $t = 1000$ time units in the experiment comprising execution time. After about 900 time units the numerical error equals the integrable one more or less, but it increases faster.

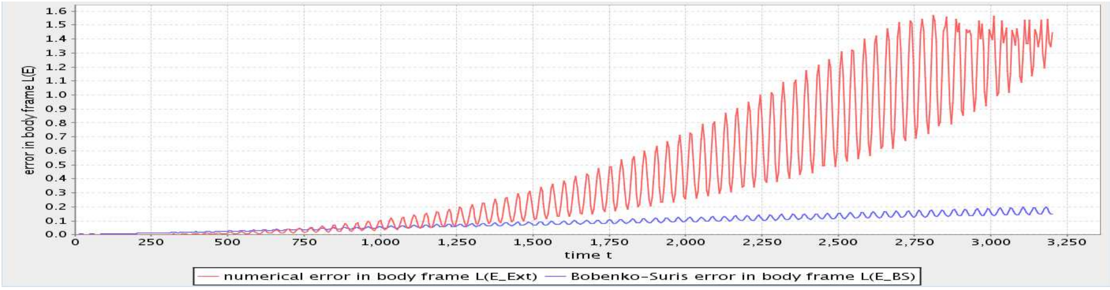

Figure 6.21: Errors in the body frame after $t = 3200$ time units in the experiment comprising execution time. The integrable discretization still yields a relatively small error, whereas the numerical error already reached the maximally possible value of $L \in [0, \frac{\pi}{2}]$.

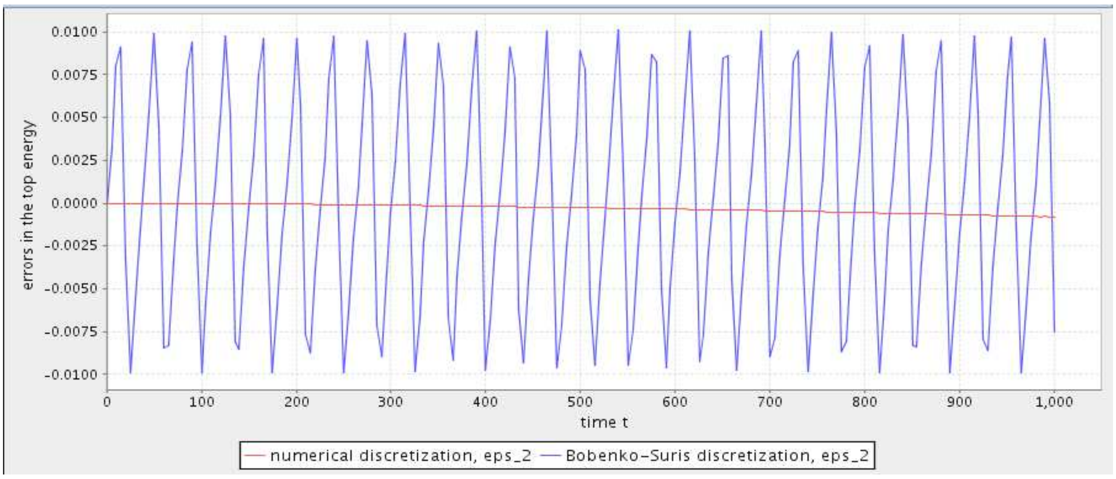

Figure 6.22: Errors in the energy after $t = 1000$ time units in the experiment comprising execution time. The error in the integrable discretization is the oscillation due to the term $\frac{\varepsilon}{2}\langle \tilde{a} \times \tilde{m}, \tilde{p} \rangle$, see section 6.1.4. The error in the numerical discretization is small but steadily increasing.

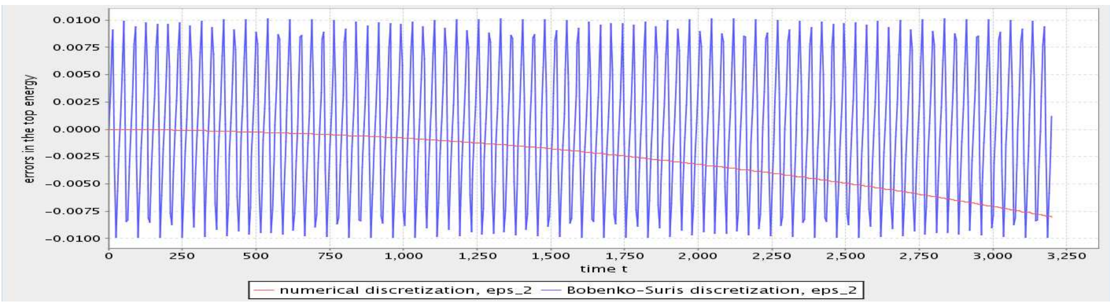

Figure 6.23: Errors in the energy after $t = 3200$ time units in the experiment comprising execution time. The numerical error reaches the magnitude of the integrable error, and keeps increasing.

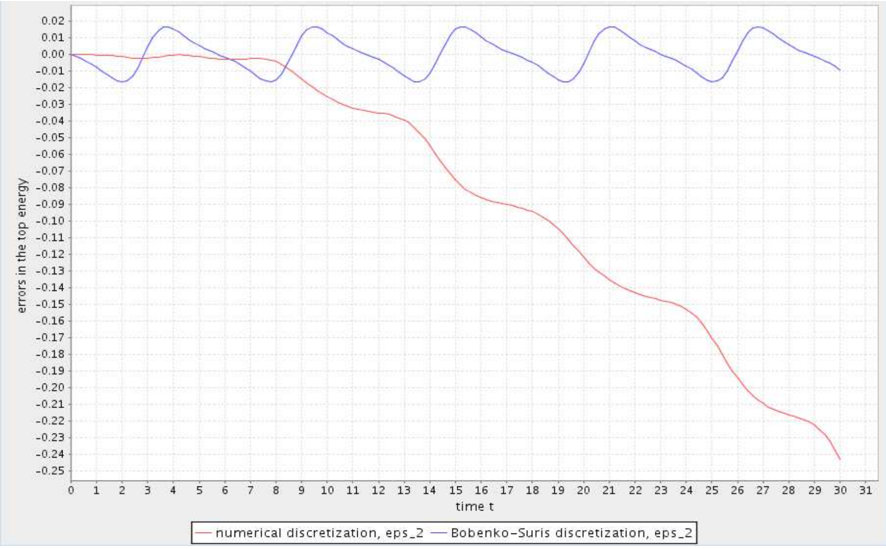

Figure 6.24: Errors in the energy after $t = 30$ time units in the experiment with comparable step sizes. The error in the *Runge-Kutta* method is small for a short time period, but increases strongly later on.

It can be observed that the error in the integrable discretization is the oscillation due to the term $\frac{\varepsilon}{2} \langle \tilde{a} \times \tilde{m}, \tilde{p} \rangle$, see section 6.1.4, and that the numerical error increases steadily. The latter is due to the fact that the local errors are transported and add up to an increasing global error.

6.3 Comparison of the *Bobenko-Suris discretization* to the *Runge-Kutta* method

The above experiments all used different step sizes in the different discretizations. For further clarification of the *Bobenko-Suris discretizations* properties now follow the results of an experiment, where the number of evaluations of the equations of motion is equal for the two discretization.

Let therefore ε_2 be the (constant) step size used in the *classical 4th order Runge-Kutta* method (*The* Runge-Kutta method). Since this is a 4 step method, i. e. the equation of motion is evaluated 4 times for doing one step, the *Bobenko-Suris discretization* works with an effective step size of $\varepsilon_2/4$, since it does so only once. The other settings are the same as in the former experiments.

Then for the experiments results with $\varepsilon_2 = 0.2$ see figures 6.24 and 6.25.

It can be observed that the *Runge-Kutta* method yields good results for a short time period. Later on, when the transported errors accumulate and amplify themselves, the results get very bad.

The same happens, just after a different amount of time, for other discretization step length parameter $\varepsilon_2 \in [0.1, 0.6]$. For larger ε_2 the results diverge very soon.

6.4 Conclusions

The *Bobenko-Suris discretization* shows both, advantages and disadvantages, compared to the numerical discretization.

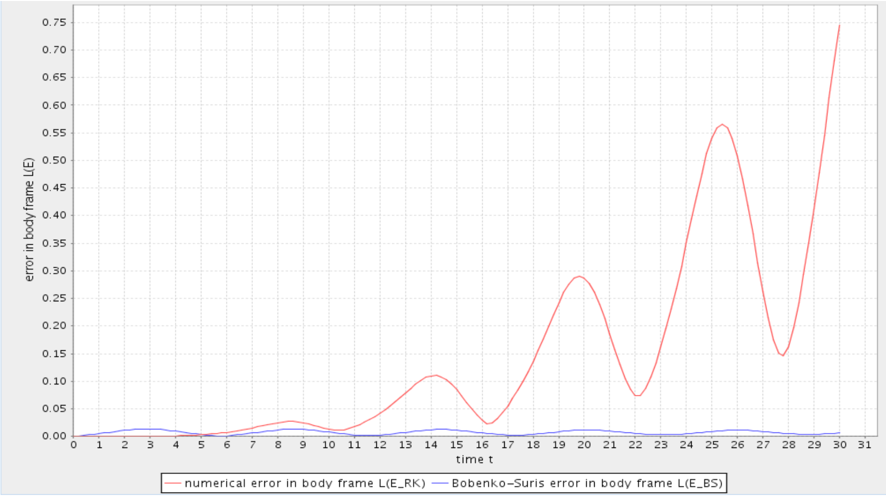

Figure 6.25: Errors in the frame after $t = 30$ time units in the experiment with comparable step sizes. Here too, the error in the *Runge-Kutta* method is small in the beginning, but grows quickly.

Mentionable disadvantages are the systematically occurring error in the energy of the top and the resulting error in the body frame already after relatively short time periods. The path of the top is a different one form the real motion. Further there is no step size control, which could make it more accurate in regions of the equations of motion with high derivatives.

Advantages are the oscillation of the error in the energy, it does not increase continuously like in numerical discretizations which makes it more suitable for long time period calculations. Further there is still a large potential in improving this discretization, e. g making it a higher order approximation or adding a step size control.

6.5 Prospects

The *Top Visualization* program was not designed for an optimized calculation of the tops paths. The experiment comprising execution time was very rough and done only for a special initial setting. A source code optimized for execution time and an application to a wider range of initial settings would surely clarify the properties of the *Bobenko-Suris discretization* more than was done in this thesis.

Further the *Bobenko-Suris discretizations* itself could be improved. As derived in [BS00] it is based on a first order discretization of the frame of an isotropic elastic rod with equidistant step sizes. It could be extended to higher order terms, and possibly even include step size control and an automatic order selection.

Appendix A

Abstract in german - Zusammenfassung auf Deutsch

Der Inhalt dieser Diplomarbeit ist ein Vergleich von Diskretisierungen der Bewegungen des Lagrange-Kreisels. Die in [BS00] entwickelte integrable Diskretisierung wird mit numerischen Lösungen verglichen, um deren Vor- oder Nachteile gegenüberzustellen. Dies geschieht mittels Implementation der verschiedenen Diskretisierungen in einem $Java^{TM}$ Programm *Top Visualization*, welches Teil dieser Diplomarbeit ist.

Dazu werden in Kapitel 2 die Grundlagen über Kreisel im Allgemeinen und den Lagrange-Kreisel im speziellen wiederholt. In Beispielen werden diese auf den Fall eines Quader angewandt, welche im *Top Visualization* Programm für die Berechnung und Visualisierung genutzt werden. Kapitel 3 befasst sich mit der kontinuierlichen Dynamik des Kreisels, Kapitel 4 mit deren Diskretisierung.

Das *Top Visualization* Programm wird in Kapitel 5 beschrieben. Es liegt der Diplomarbeit auf einer CD bei, kann aber auch im Internet unter http://www.math.tu-berlin.de/~bodack heruntergeladen oder direkt als Webstart-Applikation unter http://www.math.tu-berlin.de/geometrie/ps/software.shtml gestartet werden. Damit können die Eigenschaften des Lagrange-Kreisels selbstständig studiert und die Diskretisierungen selbst verglichen werden. Die Ergebnisse eines beispielhaften Vergleichs sind in Kapitel 6 gegeben. Desweiteren enthält Kapilel 6 die Resultate zweier zusätzlicher Experimente, die weitere Einblicke in die Eigenschaften der integrablen Diskretisierung geben. Es stellt sich heraus, dass diese Diskretisierung für Berechnungen des Kreiselpfades über kurze Zeitperioden ungeeignet ist, für längere Intervalle aber klar dominiert.

Weiterhin bietet das *Top Visualization* Programm eine Visualisierung der Bewegung von beliebigen Quadern und der intergrablen Spezialfälle des Kowalewski- und des Goryachev-Chaplygin-Kreisels. Eine kurze Beschreibung dieser Fälle findet man in Kapitel 5. Das Programm zeigt auch die Drehmoment- und Winkelgeschwindigkeitsvektoren der Kreisel, ihre Hauptträgheitsachsen und (falls diese existieren) ihre zugehörigen elastischen Stäbe. Desweiteren wird die typische Bewegung des Lagrange-Kreisels aus Präzession und Nutation mit dem sogenannten *apex trace* visualisiert.

Bibliography

[Arn] V. I. Arnold, *Mathematical methods of classical mechanics*, Springer-Verlag, Berlin, 1978.

[BBEIM] E. D. Belokolos, A. I. Bobenko, V. Z. Enol'Skii, A. R. Its, V. B. Matveev, *Algebro-Geometric Approach to Nonlinear Integrable Equations*, Springer-Verlag, Berlin, 1994.

[BS00] A. I. Bobenko and Yu- B. Suris, *A Discrete Time Lagrange Top and Discrete Elastic Curves*, Amer. Math. Soc. Transl. (2) Vol. 201, 2000.

[B97] A. I. Bobenko, *Mathematik des Kreisels*, lecture notes

[B06] A. I. Bobenko, *Differtialgeometrie von Kurven und Flächen*, http://www.math.tu-berlin.de/ bobenko/skripte.html

[HNW] E. Hairer, S. P. Norsett and G. Wanner, *Solving ordinary differential equations I. Nonstiff problems.*, 2nd edition, Springer series in computational mathematics, Springer-Verlag, 1993.

[MTJ] *Matrix Toolkits for Java (MTJ)*, http://ressim.berlios.de

[TBa] TU-Berlin, *JReality, a Java 3D Viewer for Mathematics*, http://www.jreality.de.

[TBb] TU-Berlin, *Java Tools for Experimental Mathematics*, http://www.jtem.de.